4-16-2004

Geologic Context of Geodetic Data across a Basin and Range Normal Fault, Crescent Valley, Nevada

A. M. Friedrich
California Institute of Technology

Jeffrey Lee
Central Washington University, jeff@geology.cwu.edu

B. P. Wernicke
California Institute of Technology

K. Sieh
California Institute of Technology

Recommended Citation
Friedrich, A.M., Lee, J., Wernicke, B.P., and Sieh, K. (2004). Geologic context of geodetic data across a basin and range normal fault, Crescent Valley, Nevada. *Tectonics, 23*(TC2015), 1-24. DOI: 10.1029/2003TC001528

Geologic context of geodetic data across a Basin and Range normal fault, Crescent Valley, Nevada

A. M. Friedrich[1]

Division of Geological and Planetary Sciences, California Institute of Technology, Pasadena, California, USA

J. Lee

Department of Geological Sciences, Central Washington University, Ellensburg, Washington, USA

B. P. Wernicke and K. Sieh

Division of Geological and Planetary Sciences, California Institute of Technology, Pasadena, California, USA

Received 31 March 2003; revised 16 October 2003; accepted 18 November 2003; published 16 April 2004.

[1] Geodetic strain and late Quaternary faulting in the Basin and Range province is distributed over a region much wider than historic seismicity, which is localized near the margins of the province. In the relatively aseismic interior, both the magnitude and direction of geodetic strain may be inconsistent with the Holocene faulting record. We document the best example of such a disagreement across the NE striking, ~55° NW dipping Crescent normal fault, where a NW oriented, 70 km geodetic baseline records contemporary shortening of ~2 mm/yr orthogonal to the fault trace. In contrast, our geomorphic, paleoseismic, and geochronologic analyses of the Crescent fault suggest that a large extensional rupture occurred during the late Holocene epoch. An excavation across the fault at Fourmile Canyon reveals that the most recent event occurred at 2.8 ± 0.1 ka, with net vertical tectonic displacement of 4.6 ± 0.4 m at this location, corresponding to the release of ~3 m of accumulated NW-SE extension. Measured alluvial scarp profiles suggest a minimum rupture length of 30 km along the range front for the event, implying a moment magnitude M_w of at least 6.6. No prior event occurred between ~2.8 ka and ~6.4 ± 0.1 ka, the ^{14}C calender age of strata near the base of the exposed section. Assuming typical slip rates for Basin and Range faults (~0.3 mm/yr), these results imply that up to one third, or ~1 m, of the extensional strain released in the previous earthquake could have reaccumulated across the fault since ~2.8 ka. However, the contemporary shortening implies that the fault is unloading due to a transient process, whose duration is limited to between 6 years (geodetic recording time) and 2.8 ka (the age of the most recent event). These results emphasize the importance of providing accurate geologic data on the timescale of the earthquake cycle in order to evaluate geodetic measurements. *INDEX TERMS:* 1206 Geodesy and Gravity: Crustal movements—interplate (8155); 1208 Geodesy and Gravity: Crustal movements—intraplate (8110); 7221 Seismology: Paleoseismology; 8109 Tectonophysics: Continental tectonics—extensional (0905); 8123 Tectonophysics: Dynamics, seismotectonics; *KEYWORDS:* geology, geodesy, slip rate, paleoseismology, active tectonics, multiple timescale. **Citation:** Friedrich, A. M., J. Lee, B. P. Wernicke, and K. Sieh (2004), Geologic context of geodetic data across a Basin and Range normal fault, Crescent Valley, Nevada, *Tectonics*, *23*, TC2015, doi:10.1029/2003TC001528.

1. Introduction

[2] Do geodetic measurements across wide plate boundary regions record steady state, long-term elastic strain accumulations across individual faults? While geodetic measurements across plate boundary regions generally match long-term geologic measurements (e.g., NUVEL 1A [*DeMets et al.*, 1994]; REVEL [*Sella et al.*, 2002]), for a number of major fault zones, it is controversial as to whether geodetic and geologic rates are in agreement. For example, the Holocene displacement rate across the western Garlock fault in southern California is 7 mm/yr [*McGill and Sieh*, 1993], whereas the geodetic rate measured over the last 10 years shows little or no left-lateral shear strain across the fault [*Miller et al.*, 2001; *Peltzer et al.*, 2001]. Similarly, the late Quaternary displacement rate across the central Altyn Tagh fault zone in Asia is near 30 mm/yr [*Meriaux et al.*, 2000], but regional geodetic data from central Asia suggest that the rate can be no more than 10 mm/yr [*Wang et al.*, 2001]. In eastern California, the Holocene displacement rate on the Owens Valley fault appears to be about a factor of 2 less than the contemporary geodetic rate, based on simple elastic dislocation models [*Lee et al.*, 2001; *Dixon et al.*, 2003]. Explanations for disagreements between geodetic rates and geologic fault slip rates involve short-term, quasi-periodic transients related to earthquakes, slip accommodated along structures not yet identified [e.g., *Lee*

[1]Now at Institute of Geosciences, University of Potsdam, Golm, Germany.

0278-7407/04/2003TC001528$12.00

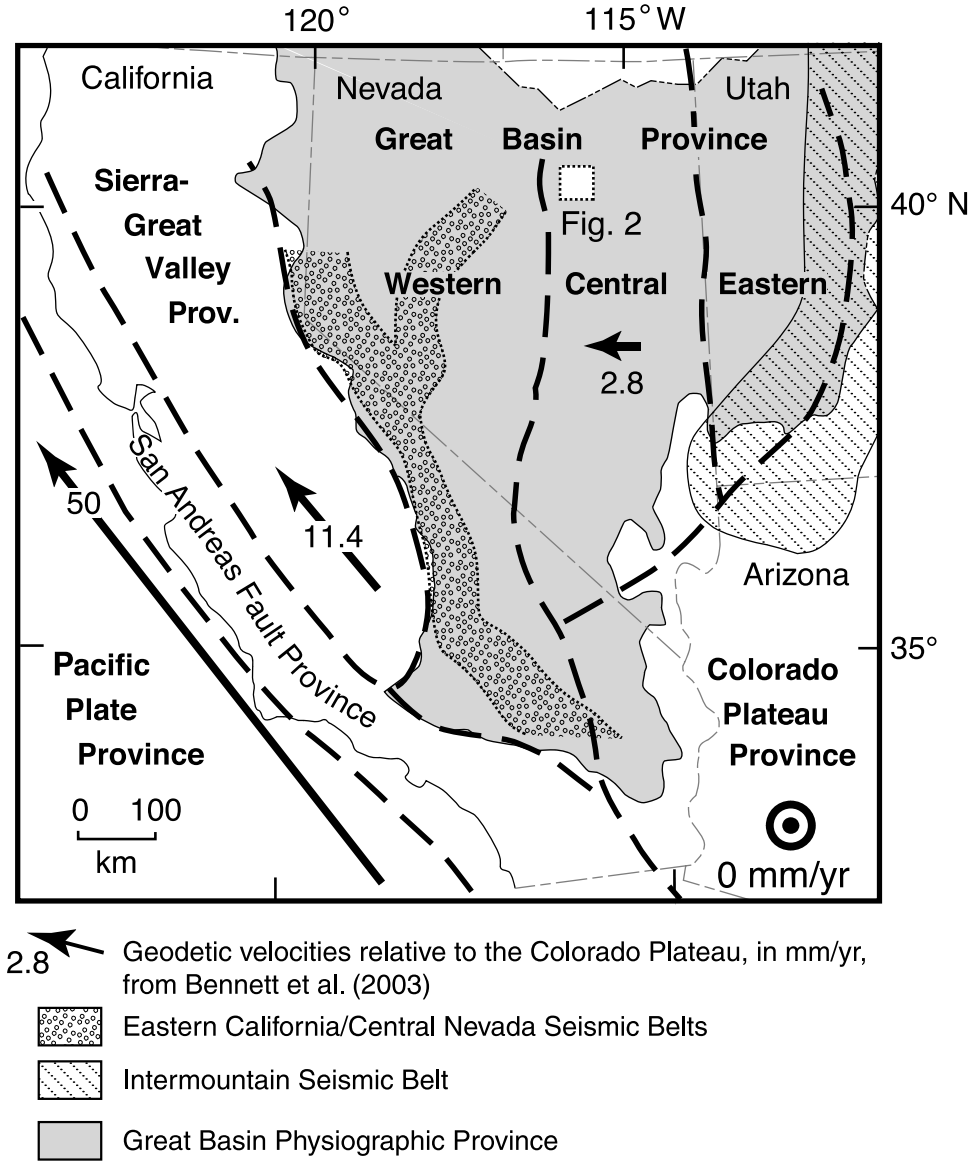

Figure 1. Map showing geodetic provinces of the western United States from *Bennett et al.* [2003], depicting motions of relatively little-deformed blocks (arrows) with respect to the Colorado Plateau province, and location of Figure 2. Principal belts of seismicity in the Great Basin/Colorado Plateau region shown with stipple patterns.

et al., 2001], or to activation and deactivation of faults [e.g., *Peltzer et al.*, 2001]. In these cases and others, the reported discrepancies are of the same order of magnitude and of the same sign as the measurements themselves.

[3] Earlier, we reported geodetic data from a continuous GPS baseline across the Crescent fault in north central Nevada, a typical Basin and Range normal fault, indicating horizontal shortening oriented normal to the trace of the fault of ~2 mm/yr [*Wernicke et al.*, 2000]. Given the typical long-term displacement rates across Basin and Range normal faults of ~0.2–0.4 mm/yr [e.g., *Thompson and Burke*, 1973; *Bennett et al.*, 1999; *Davis et al.*, 2003], neither the magnitude nor the sign of the geodetic measurement agreed with the presumed geological rate. The seismic history of the Crescent fault is therefore of great interest, because it would limit the timescale over which shortening could have occurred, and establish the context of geodetic measurements in the seismic cycle of the Crescent fault. Here we report results from geomorphic and paleoseismological investigations of the Crescent fault and discuss their implications for models of fault system dynamics.

2. Neotectonic Setting of the Northern Basin and Range

[4] The northern Basin and Range province is a ~800 km wide region of continental extension between

the Sierra Nevada and the Colorado Plateau (Figure 1). At any latitude, the province consists of ~20, mostly north to NNE striking Quaternary normal faults that separate footwalls of east or west tilted horsts from shallow (1–4 km) basins with a typical relief of ~1500 m [e.g., *Stewart*, 1971, 1978]. Offset late Quaternary sedimentary and volcanic deposits indicate that most normal faults have ruptured the surface at least once during late Quaternary time [e.g., *Dohrenwend et al.*, 1996; *Hecker*, 1993]. The latest snapshot of activity is recorded by historic seismicity in narrow belts near the margins of the province, including the Central Nevada and Eastern California Seismic Belts on the west and the Intermountain Seismic Belt on the east (Figure 1). In both of these belts, late Holocene (<2500 years) surface ruptures have been documented [e.g., *Wallace*, 1977; *Machette et al.*, 1992a, 1992b; *Caskey et al.*, 1996; *Bell et al.*, 1999; *Lee et al.*, 2001]. Earthquakes in the Intermountain Seismic Belt generally occur on north striking normal faults [e.g., *Arabasz et al.*, 1980; *Doser and Smith*, 1982], whereas earthquakes in the Eastern California Seismic Belt occur predominantly on NNW striking right-lateral strike-slip faults. To the north, in the Central Nevada Seismic Belt, earthquakes show a transition from right-lateral strike slip in the south to nearly pure normal motion farther north [e.g., *Smith and Sbar*, 1974; *Caskey et al.*, 1996].

[5] On the basis of regional neotectonic analyses of Crescent Valley and environs, which included measurements of the orientations and slip directions on active faults, the late Cenozoic stress regime is one of pure normal faulting, with the least principal stress direction oriented N40–80°W (Figure 2) [*Zoback and Thompson*, 1978; *Zoback and Zoback*, 1980; *Zoback*, 1989; *Zoback et al.*, 1994].

[6] The present-day deformation pattern in the Great Basin region is constrained by both campaign and continuous GPS data, which define "geodetic provinces" of internally uniform deformation pattern [*Bennett et al.*, 2003]. Bounding the Great Basin region to the east and west are the internally stable Colorado Plateau and Sierra Nevada/Great Valley provinces, respectively (Figure 1). The Sierra Nevada/Great Valley province is moving 11.4 mm/yr N47°W relative to the Colorado Plateau province (Figure 1). Between them, the Great Basin contains three provinces: the western, central, and eastern Great Basin provinces (Figure 1). Most or all of the northerly motion of the Sierra Nevada/Great Valley province is accommodated via nearly pure, N37°W right-lateral shear of 9.3 mm/yr across the western Great Basin province, whereas the remaining westward motion of ~2.8 mm/yr is more broadly distributed across the eastern Great Basin province [*Bennett et al.*, 2003]. Overall, the central Great Basin province has a negligible average strain rate, but contains several baselines indicating significant local shortening or extension (Figure 2) [*Wernicke et al.*, 2000, Figure 1; *Bennett et al.*, 2003].

[7] The Crescent Valley area lies near the western margin of the central Great Basin province (Figure 1), where shortening, at a rate of 1.8 ± 0.1 mm/yr in a N46°W direction, is most pronounced across the baseline LEWI-MINE (Figure 2) [*Wernicke et al.*, 2000].

3. Geologic Setting of the Crescent Valley Region

[8] The ~60 km long, ~55°NW dipping Crescent fault lies astride the LEWI-MINE baseline (Figure 2). Its strike is roughly perpendicular to the baseline, and it is the only major Late Quaternary fault that crosses the geodetic baseline, although other faults are present not far east of MINE and west of LEWI [e.g., *Dohrenwend et al.*, 1996]. The Crescent fault separates the Cortez Mountains block to the southeast from the Shoshone Range and Dry Hills blocks to the northwest. To the south, the fault appears to transfer much of its displacement onto the Cariko Lake faults in the southwest and the Cortez-Grass Valley faults along the southernmost portion of the Cortez Range, whereas to the north slip apparently dies out (Figure 2).

[9] The mountain ranges in the area are capped by gently SE dipping ~14 Ma mafic volcanic rocks [*Gilluly and Masursky*, 1965]. In the southern Cortez Mountains, they project westward to intersect the fault plane ~1 km above the valley floor [*Gilluly and Masursky*, 1965]. Quaternary deposits in the hanging wall of the Crescent Valley fault are estimated to be ~2 km thick, on the basis of gravity data [*Gilluly and Gates*, 1965; *Gilluly and Masursky*, 1965]. This is approximately the depth at which the basalt flows on the Shoshone range block would intersect the Crescent fault if projected beneath the valley fill. Assuming that displacement along the fault entirely postdates the extrusion of the volcanic flows, these data imply a cumulative vertical displacement of ~3 km along the southern Crescent fault.

4. Quaternary History of the Crescent Fault

[10] Along most of its trace, the Crescent fault juxtaposes pre-Tertiary bedrock in the footwall with Quaternary alluvial fan and interfan colluvial aprons in the hanging wall (Figures 3 and 4a). The footwall of the Crescent fault exhibits some of the best examples of faceted spurs in the Basin and Range province (Figures 3 and 4b). The best exposure of the Crescent fault occurs in a ~20 m high quarry wall at the Cortez mine (Figure 4a), There the fault dips 55°NW and juxtaposes Quaternary alluvium against Mesozoic intrusive rocks (Figure 4c).

[11] Alluvial fan surfaces, with local fan-head elevation differences of up to 15 m define several periods of deposition along the range front (Figure 3). The oldest and highest surface, Pf1, has a well-developed desert pavement, a prominent carbonate-enriched (B_k) soil horizon, and in places is cut by latest Pleistocene/early Holocene shorelines [*Reheis*, 1999]. Near the range front, Pf1 is covered by colluvial deposits that conceal any interactions with the fault. The next younger surface, Hf2, is extensively exposed along the range front where canyons and creeks debouch into Crescent Valley. This surface contains numerous scarps along the trace of the Crescent fault (Figures 3, 4a, and 4b).

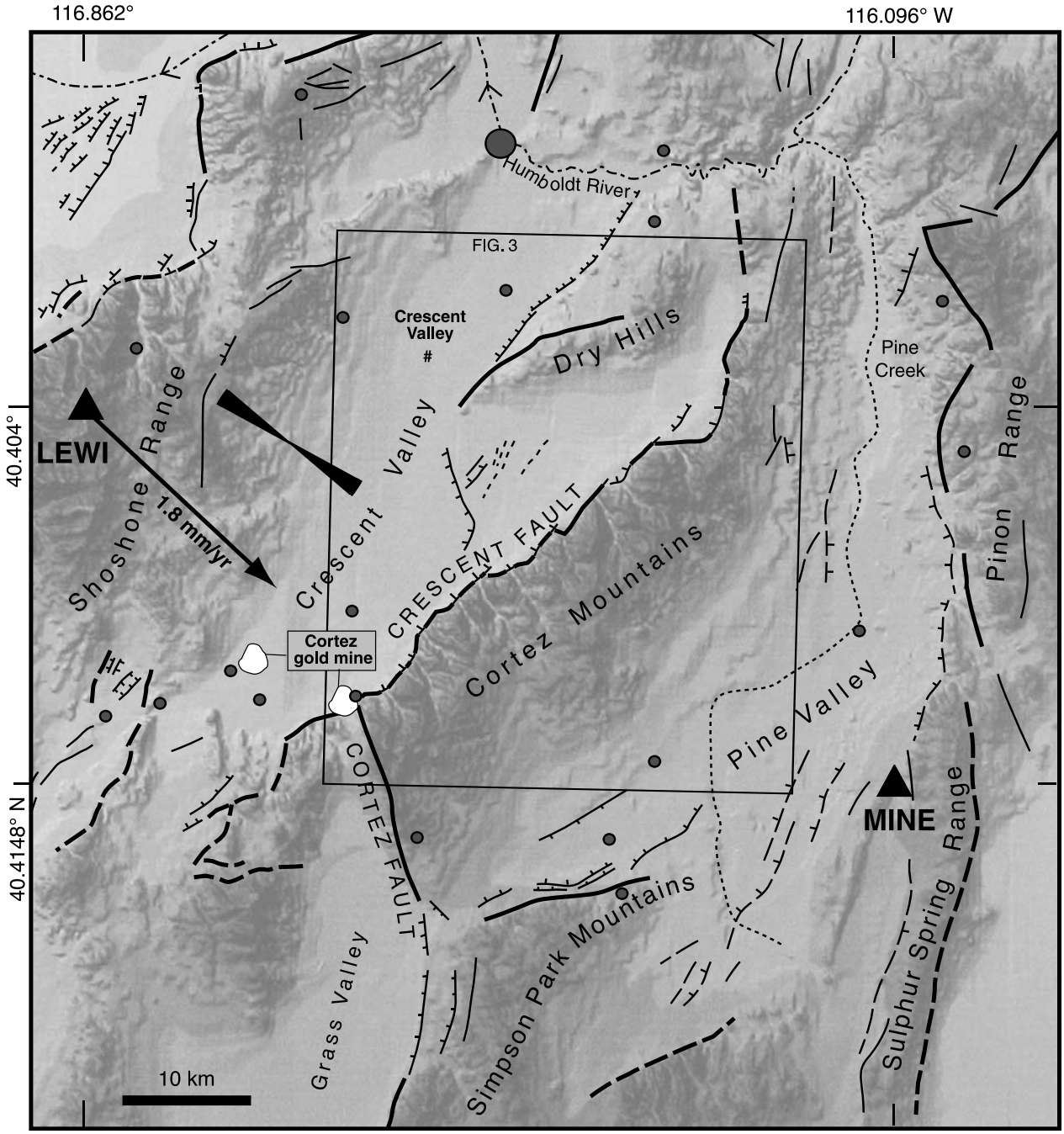

Figure 2. Shaded DEM of the Crescent region showing positions of Quaternary fault scarps [from *Dohrenwend et al.*, 1996], historic seismicity, the continuous geodetic sites, and the regional stress field. Note that the measured geodetic velocity (arrow) differs in sign, or by 180°, from the expected extension direction based on orientation of normal faults [*Dohrenwend et al.*, 1996] and the least principal stress direction based on fault slip data in the area (bow tie symbol [e.g., *Zoback*, 1989]). Other symbols are as follows: thick lines, bedrock footwalls; thin lines, alluvial footwalls; triangles, positions of BARGEN continuous GPS sites; arrow, velocity of site LEWI relative to MINE [*Wernicke et al.*, 2000];circles, epicenters of known earthquakes 1852–1996 with $M < 4$ (small circles) and $4 < M < 5$ (large circle [*dePolo and dePolo*, 1999].

Figure 3. Simplified neotectonic map of the Cortez Mountains range front showing the traces of the Crescent and surrounding normal faults, distributions of bedrock (light gray uplands) and major alluvial and lacustrine deposits, and the distribution and slope of faceted spurs in the footwall of the Crescent fault. The most recent rupture occurred along the southern segment of the Crescent fault, where alluvial fans are small and the range front sinuosity is low.

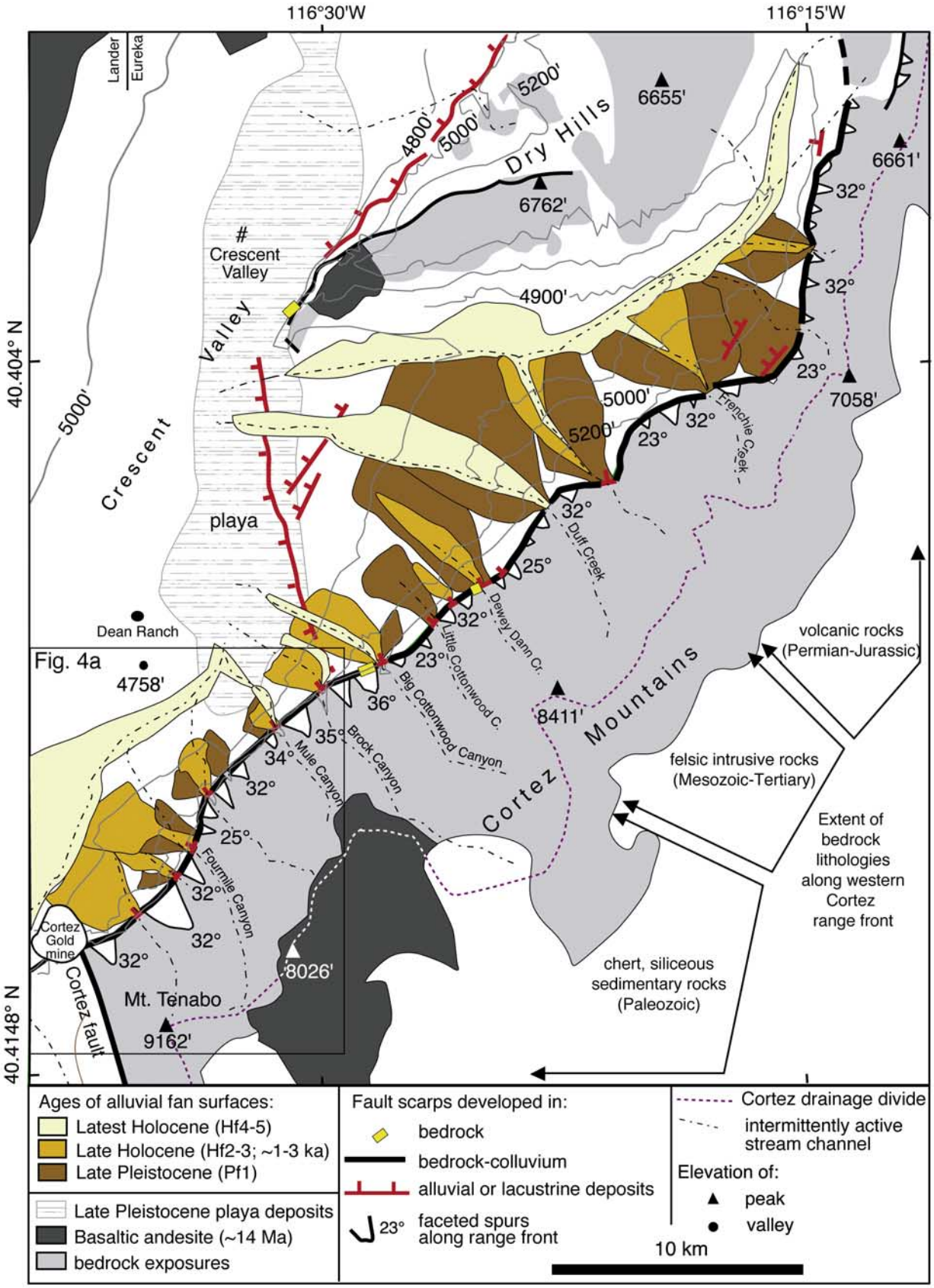
116°30'W
116°15'W
40.404° N
40.4148° N
Lander
Eureka
Dry Hills
6655'
6661'
6762'
4800'
5000'
5200'
Crescent Valley
4900'
7058'
Frenchie Creek
Duff Creek
Dewey Dann Cr.
Little Cottonwood C.
Big Cottonwood Canyon
Brock Canyon
Mule Canyon
Fourmile Canyon
Dean Ranch
Fig. 4a
4758'
playa
8411'
Mountains
Cortez
Cortez Gold mine
Cortez fault
Mt. Tenabo
9162'
8026'
volcanic rocks (Permian-Jurassic)
felsic intrusive rocks (Mesozoic-Tertiary)
Extent of bedrock lithologies along western Cortez range front
chert, siliceous sedimentary rocks (Paleozoic)
Ages of alluvial fan surfaces:
Latest Holocene (Hf4-5)
Late Holocene (Hf2-3; ~1-3 ka)
Late Pleistocene (Pf1)
Late Pleistocene playa deposits
Basaltic andesite (~14 Ma)
bedrock exposures
Fault scarps developed in:
bedrock
bedrock-colluvium
alluvial or lacustrine deposits
faceted spurs along range front
Cortez drainage divide
intermittently active stream channel
Elevation of:
peak
valley
10 km

Figure 3.

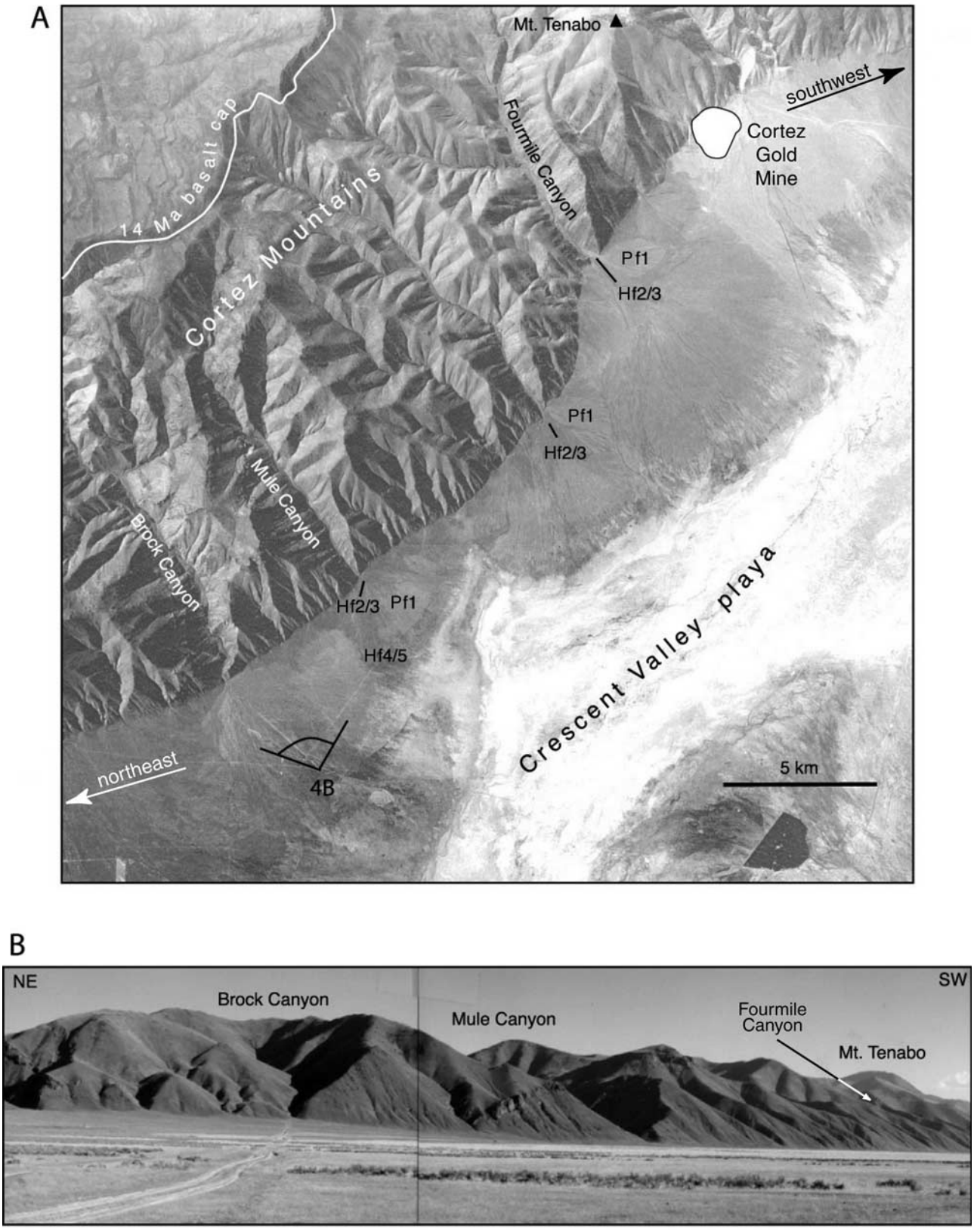
A
Mt. Tenabo
southwest
Cortez
Gold
Mine
Fourmile Canyon
14 Ma basalt cap
Cortez Mountains
Pf1
Hf2/3
Pf1
Hf2/3
Mule Canyon
Brock Canyon
Hf2/3 Pf1
Hf4/5
Crescent Valley playa
northeast
4B
5 km
B
NE
SW
Brock Canyon
Mule Canyon
Fourmile
Canyon
Mt. Tenabo

Figure 4.

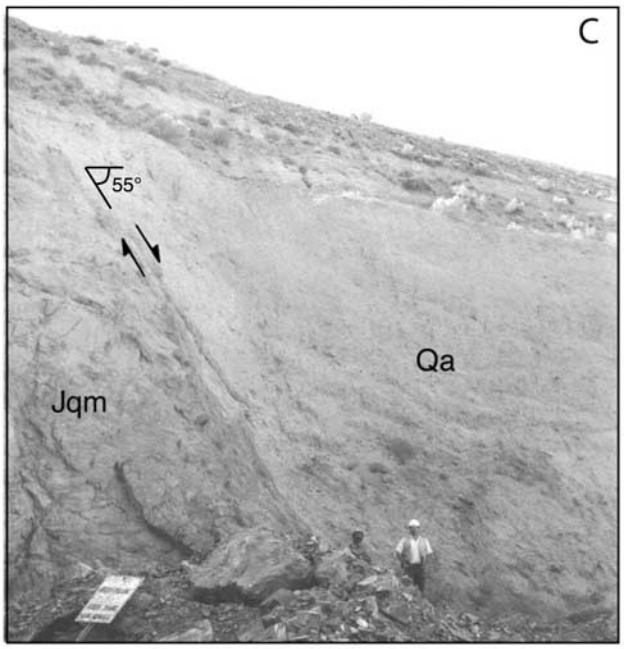

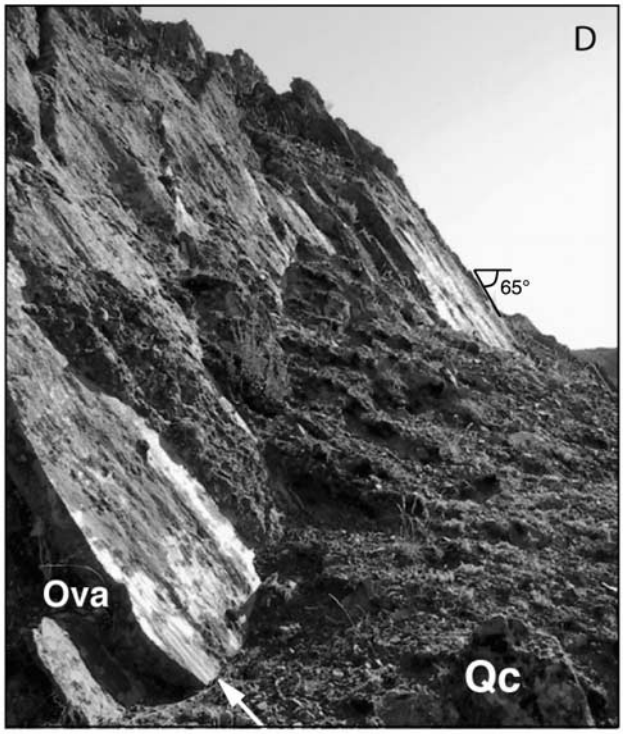

Figure 4. (continued)

This surface has not developed pavement, and does not have a well-developed B_k horizon. We show below that this surface formed in the Late Holocene. The next younger surface, Hf3, is not cut by the fault and overlaps Hf2 on the hanging wall block of the fault. The youngest major surface, Hf4, is present primarily along active drainages and also overlaps the Crescent fault. The active washes contain between one and three additional terrace levels younger than Hf4, which we have grouped as Hf5.

[12] The range front morphology varies along strike of the Crescent fault. In the southwest, the range front is characterized by relatively tall, steep triangular facets and relatively small, low relief (~50–150 m head-to-toe elevation difference) alluvial fans (Figures 3, 4a, and 4b). In the northeast, particularly north of Little Cottonwood Canyon, the triangular facets are generally smaller and less steep, landslides are frequent, and Pf1 alluvial fans are larger and have higher relief (~300 m), implying relatively high erosion rates. This change corresponds to a difference in bedrock composition from predominantly siliceous Paleozoic strata to the southwest to predominantly Mesozoic volcanic rocks to the northeast. It is uncertain, however, to what degree either one or both of these differences reflect a northward increase in bedrock erodability or a northward decrease in exhumation along the Crescent fault. In addition, the Crescent fault appears to splay northward into at least two branches, one of which bounds the Dry Hills and the other the Cortez Mountains (Figure 3). Because of this complexity, we have targeted our paleoseismological investigations along the southwestern portion of the Crescent fault.

5. Character of Fault Scarps

[13] The Crescent fault most commonly juxtaposes bedrock and interfan colluvial deposits that onlap bedrock and conceal the fault trace. However, in two localities along the range front (Big Cottonwood and Dewey Dann creeks), prominent bedrock scarps are exposed above the colluvial mantle (Figure 3). The scarps are exposed for tens of meters along strike of the fault and are locally up to 6 m high. They are developed on tabular zones of silicification parallel to the fault and display a high degree of polish, especially along their bases (Figure 4d). Both scarps dip steeply (55–65°NW) and exhibit well developed, steeply plunging striations with rakes of ~70° (Figure 4d).

[14] At the mouths of most creeks and canyons, the heads of Hf2 surfaces are cut by the Crescent fault scarp (Figure 3). The Hf2 fan aprons are likewise cut by a series of relatively small scarps (~1 m vertical offset) that diverge northward

Figure 4. (a) Aerial photograph showing the trace of the Crescent fault (solid arrows) from the Cortez Gold Mine to Brock Canyon. Note low sinuosity of range front. See Figure 3 for location. (b) Photograph looking southeast toward Mule Canyon (right-center) from Crescent Valley, showing the trace of the Crescent fault and conspicuous faceted spurs. Note rise of fan heads northeastward (to the left). See Figure 4a for location. (c) Photograph looking southwest toward exposure of Crescent fault in Cortez Gold Mine; Jqm, Jurassic quartz monzonite; Qa, Quaternary alluvium. Note geologists for scale. (d) Photograph looking southwest toward bedrock scarp exposure of Crescent fault just southwest of Big Cottonwood Canyon, showing slickensides and fault striations (arrow); Ova, Ordovician Valmy Formation; Qc, Quaternary colluvial deposits. Scarp height in photo is about 1.5 m.

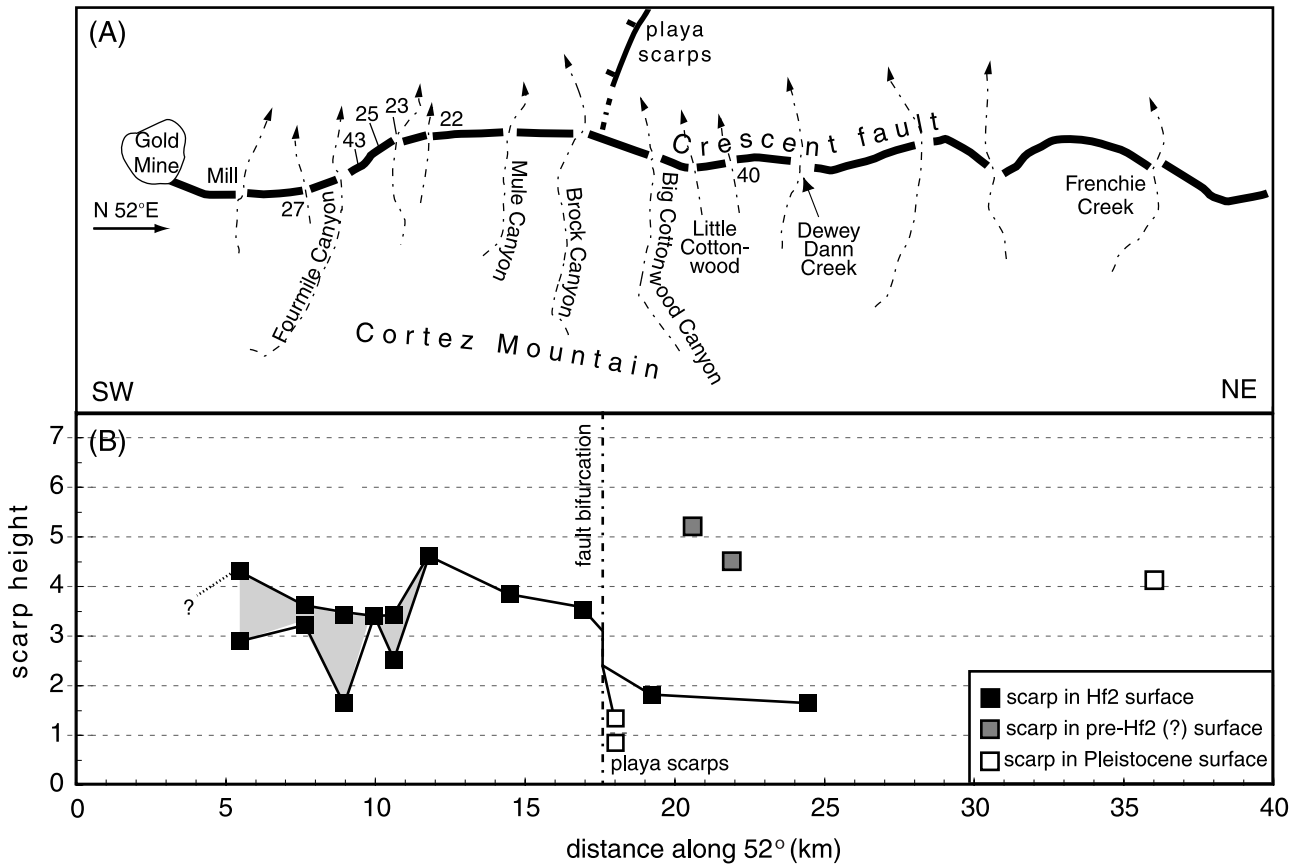

Figure 5. (a) Trace of Crescent fault (thick line) and principal drainages crossing the fault (dashed lines with arrows) and the positions of alluvial scarp profiles (Figure 7a) used to determine offsets of the Hf2 surface shown in Figure 5b. Numbers show locations where unnamed drainages intersect the fault. (b) Offsets of Hf2 surface along the range front, from scarp profiles shown in Figure 7a and auxiliary material. Note the sudden decrease in displacement across the playa splay faults.

from the Crescent fault toward the Dry Hills (Figure 3). Pf1 fan deposits rarely show any fault offsets, but north of Frenchie Creek, a ~4 m offset is preserved (Figure 5b).

[15] We measured topographic profiles of the Hf2 surface scarps using a theodolite. At each canyon mouth, we measured the profiles perpendicular to the strike of the fault scarp at the location along strike where the thickness of overlying younger deposits on the hanging wall block is minimized (see auxiliary material[1]). These profiles show net vertical tectonic displacements (NVTD) [*Witkind et al.*, 1964] that range from 1.5 to 5.2 m (Figures 5 and 6); however, in many instances a difference in slope between hanging wall and footwall surfaces implies that the hanging wall surface is not the same as that of the footwall (Figure 6 and auxiliary material[1]). These differences in slope generally reflect the observation that the Hf2 surface is well defined in the footwall but tends to be concealed beneath younger deposits in the hanging wall. Therefore the scarp profile offsets are generally a minimum estimate of the net offset of Hf2.

[16] The Hf2 scarp profiles are not composite scarps (Figure 6a), implying that the offset occurred as the result of either a single event or multiple events closely spaced in time. The Hf2 scarp profiles form an array on a measured scarp height versus maximum slope angle plot [*Bucknam and Anderson*, 1979] comparable with other arrays of such data from Holocene fault scarps (Figure 6b). The displacement profiles of Hf2 scarps, along strike of the Crescent fault (Figure 5b), appears to be similar in magnitude and variability to profiles measured on fault scarps produced by historic earthquakes in the Basin and Range (e.g., maximum displacements are as follows: Dixie Valley, 3.8 m, 45 km

Figure 6. (a) Measured alluvial scarp profiles. The auxiliary material contains detailed diagrams showing graphical determinations of minimum net vertical tectonic displacement for each profile. (b) Graph of scarp height versus scarp slope angle for Crescent fault Hf2 alluvial scarps. Data trends for comparison include the late Holocene Fish Springs (~2 ka), earliest Holocene Drum Mountains (~10 ka) and late Pleistocene Panguitch (~100 ka) scarps [*Bucknam and Anderson*, 1979] (ages from *Machette et al.* [2001]).

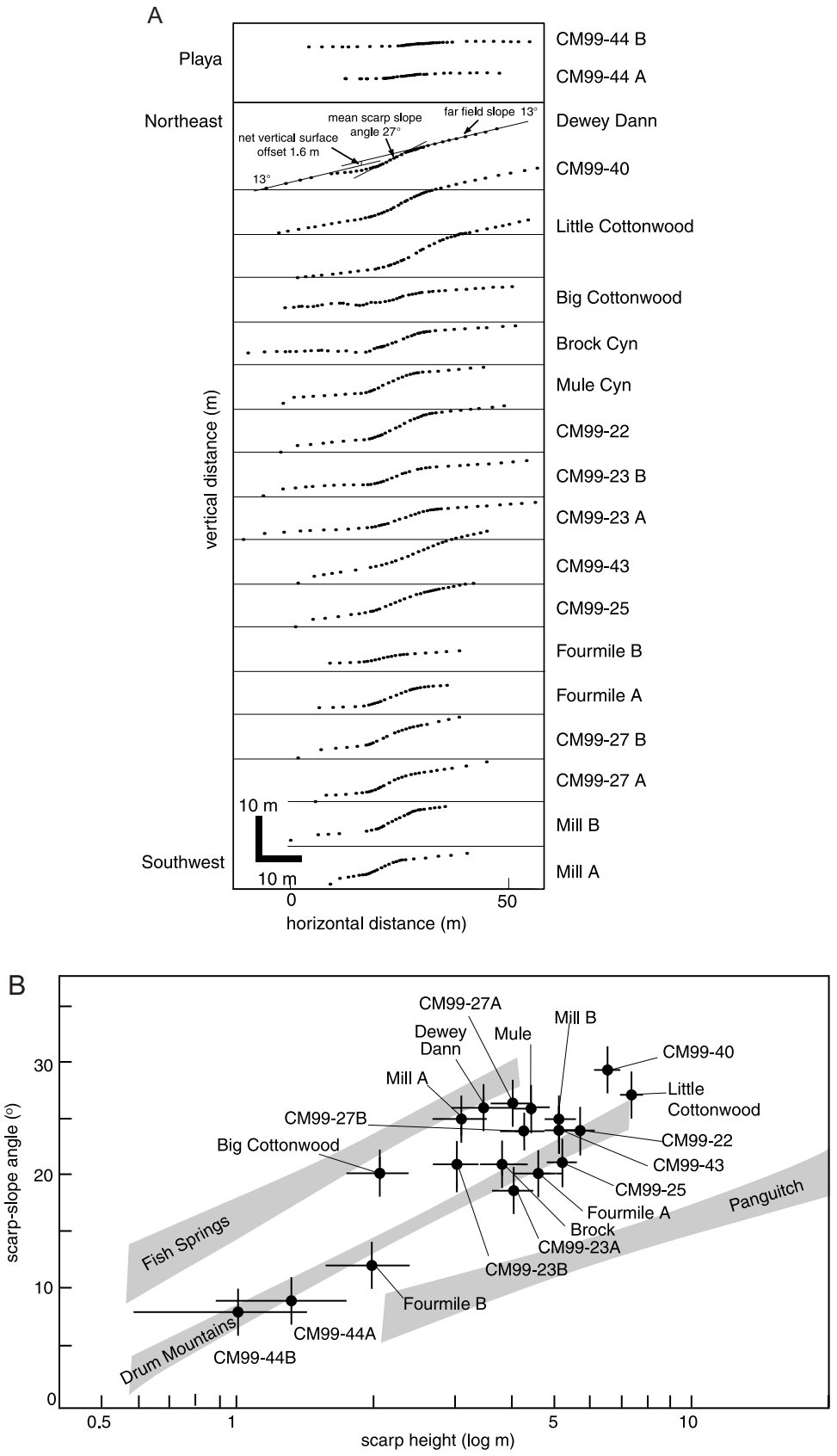
A
Playa
Northeast
Southwest
CM99-44 B
CM99-44 A
Dewey Dann
CM99-40
Little Cottonwood
Big Cottonwood
Brock Cyn
Mule Cyn
CM99-22
CM99-23 B
CM99-23 A
CM99-43
CM99-25
Fourmile B
Fourmile A
CM99-27 B
CM99-27 A
Mill B
Mill A
mean scarp slope angle 27°
far field slope 13°
net vertical surface offset 1.6 m
13°
10 m
10 m
vertical distance (m)
0
50
horizontal distance (m)
B
CM99-27A
Mill B
Dewey Dann
Mule
CM99-40
Mill A
Little Cottonwood
CM99-27B
CM99-22
Big Cottonwood
CM99-43
CM99-25
Fourmile A
Brock
CM99-23A
CM99-23B
Fourmile B
CM99-44A
CM99-44B
Fish Springs
Drum Mountains
Panguitch
scarp-slope angle (°)
0
10
20
30
0.5
1
5
10
scarp height (log m)

Figure 6.

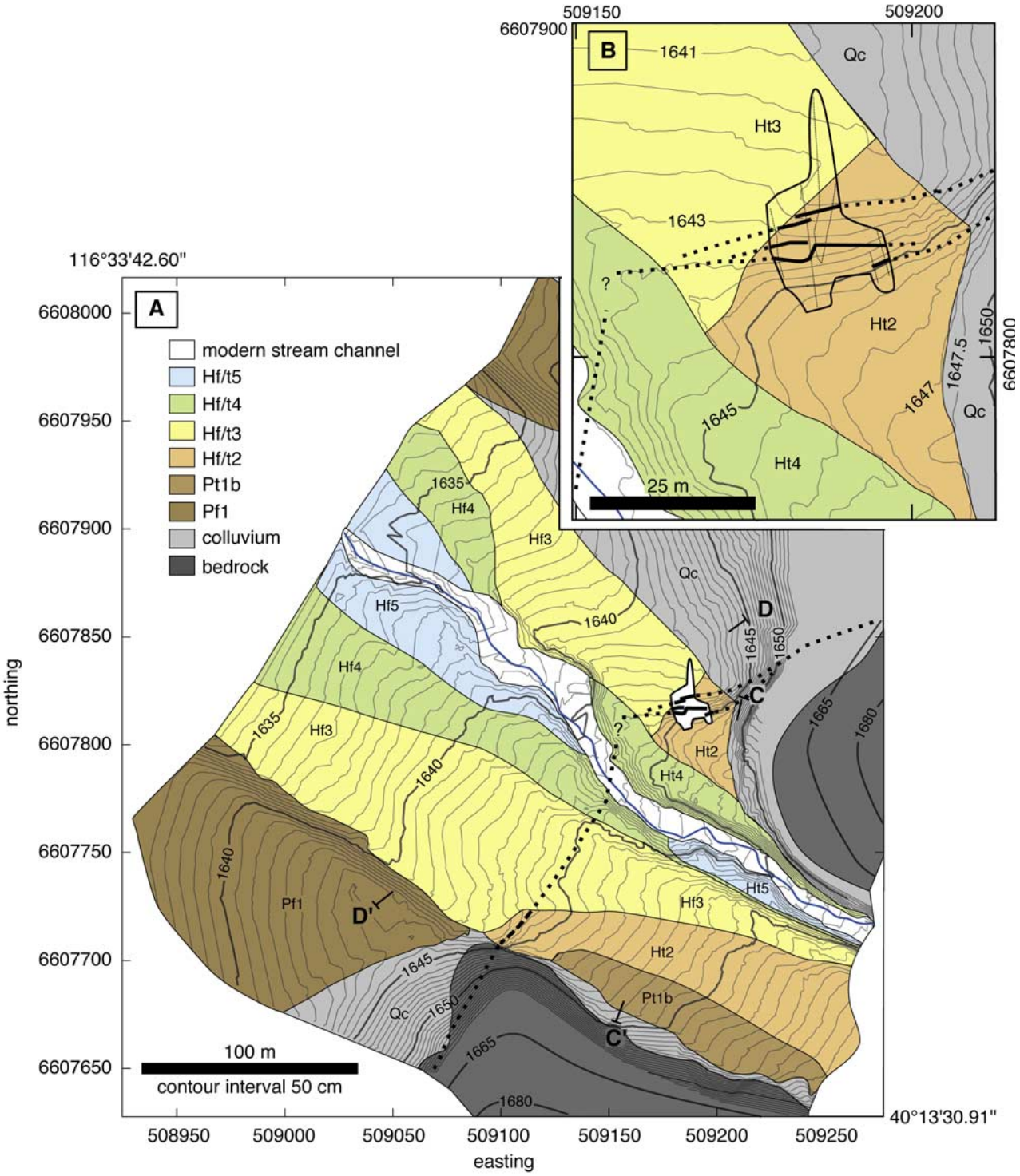

Figure 7. (a and b) Surficial geologic map of the Fourmile Canyon area, distinguishing bedrock, colluvial deposits, various river terraces and alluvial fan deposits. Small, irregular white patch north of the canyon shows our excavation across the Crescent fault. Fault is dashed where approximately located, dotted where concealed. Topographic contour interval is 50 cm, except where contours are omitted in steep terrain. (c and d) Cross sections of surficial deposits in footwall and hanging wall of Crescent fault, respectively, with the approximate outlines of the final excavation. Note the continuous deposition of Hf2 and Hf3 fill in the hanging wall section (Figure 7d), in contrast to the footwall section (Figure 7c) with incision into the Hf2 surface and formation of a strath terrace as a response to displacement-related footwall erosion.

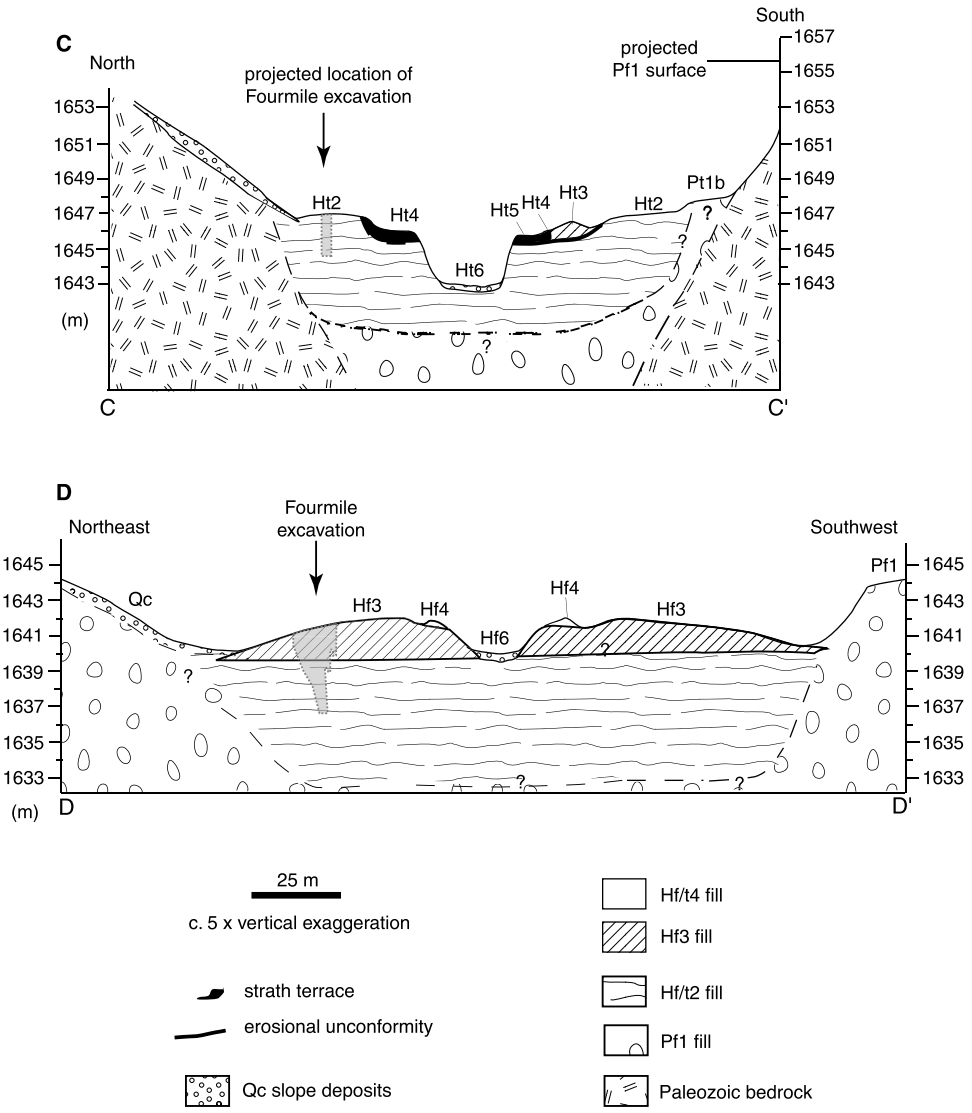

Figure 7. (continued)

rupture length, and Fairview Peak, 4.8 m, 67 km rupture length [*Slemmons*, 1957]; Hebgen Lake, 6.1 m [*Myers and Hamilton*, 1964]; Pleasant Valley, 5.8 m, 59 km [*Wallace*, 1977, 1984a, 1984b]; Borak Peak, 2.7, 34 km [*Crone et al.*, 1987]; Edgecumb, 2.9 m, 18 km [*Beanland et al.*, 1990]) [*Caskey et al.*, 1996].

6. Paleoseismology of the Fourmile Canyon Area

[17] To determine an age and maximum vertical displacement of a typical Hf2 surface, we chose to study the scarp at Fourmile Canyon by excavating an outcrop of these deposits (Figure 3). The scarp at Fourmile Canyon is well suited for such a study because (1) it occurs along the relatively simple southwestern segment of the Crescent fault system (Figure 4); (2) offset of the Hf2 surface is relatively large and well defined (Figure 6); (3) the alluvial fan at the mouth of Fourmile Canyon has been aggradational both before and after the time of the last offset, which provides a detailed stratigraphic record at the time of faulting [cf. *Grant and Sieh*, 1994], (4) the fault scarp and its colluvial apron are partially overlapped by Hf3 alluvial deposits, preserving its morphology in the subsurface and providing an opportunity to constrain the minimum age limit for offset of the Hf2 surface, and (5) Fourmile Canyon drains a forested portion of the Cortez Mountains, which provides an excellent source of charcoal for relatively precise radiometric dating of the sedimentary record.

6.1. Alluvial History

[18] Fourmile Creek is one of the largest drainages of the southern Cortez Mountains. Six geomorphic surfaces record the recent fluvial history at the mouth of the canyon (Figures 7 and 8). We made a detailed topographic map of these surfaces and the fault scarp using closely spaced

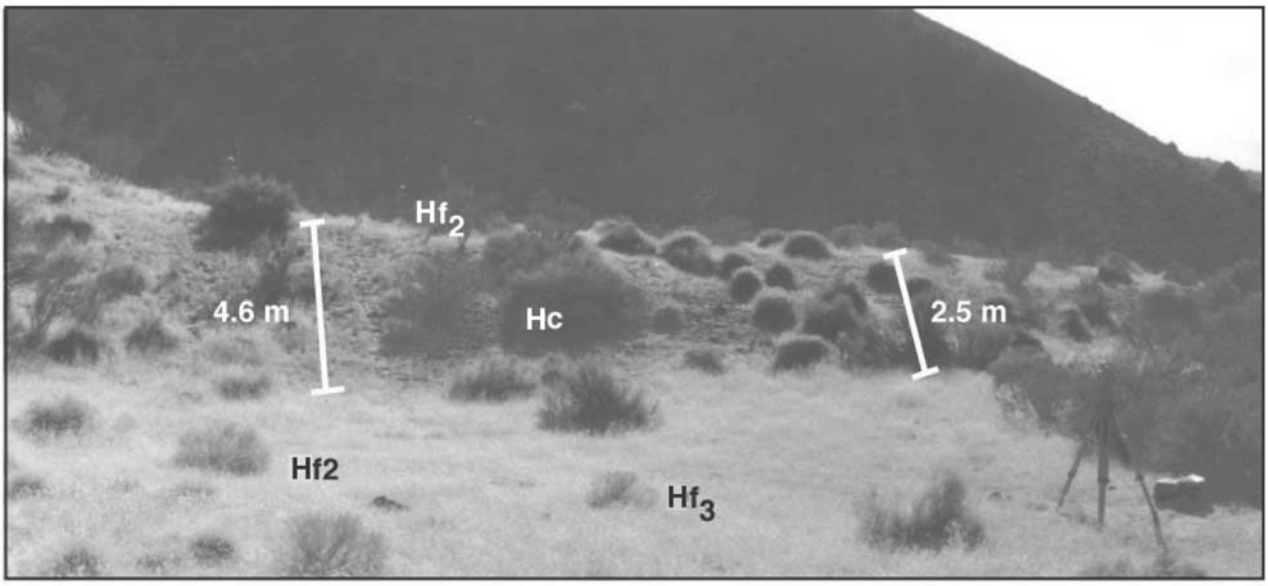

Figure 8. Photograph looking southeast at fault scarp in alluvium just north of Fourmile Canyon prior to excavation, showing offset Hf2 surface and overlap of scarp by Hf3 deposits.

(<0.5 m) points obtained with differential Global Positioning System equipment, which served as a base for mapping the individual surfaces (Figures 7a and 7b). Our convention is to designate those surfaces downstream from the fault with the letter f (fan surface) and those on the upstream side with the letter t (fluvial terrace). Following the letter designation, we assign a number or a number and a letter to indicate relative age.

[19] The oldest surface, Pf1, is preserved only downstream of the fault, and is continuously exposed for several kilometers down fan (Figures 3 and 7a). The next youngest surface, Pt1b, occurs only on the south side of the canyon upstream of the fault, several meters below the projection of surface Pf1 (Figures 7a and 7c). Although we lack an exposure, we interpret it as a strath terrace cut in either colluvium or fan deposits Pf1. We cannot rule out the possibility, however, that it represents a fill terrace intermediate in age between Pf1 and Hf2. The next youngest surface, Ht2/Hf2, is the top of an alluvial fill that our excavations show to be exposed upstream from the fault and buried downstream. The next youngest surface, Ht3, is also a fill terrace that is contiguous across the fault, from the Hf3 fan surface to >100 m up canyon. Ht3 filled a channel incised into the footwall block after the fault offset the Ht2/Hf2 surface. Thus, downstream of the fault, Ht3 represents an alluvial wedge deposited conformably on Hf2 and buttressed against the fault scarp, whereas on the footwall it fills a channel cut into Ht2 (Figures 7c and 7d).

[20] Following aggradation to the Ht3/Hf3 deposit, the stream cut two strath terraces, Ht4 and Ht5, into the older deposits (Figure 7a). These two surfaces persist as straths only a short distance downstream before they become indistinguishable with the Hf3 surface. The active channel, Ht6, is 10–30 m wide, and does not markedly change its width nor gradient in the vicinity of the fault. Thus, unlike the distributary geometry of surface Hf3, the youngest surface is channelized well down fan of the fault. These observations imply that the active stream-fan system has re-equilibrated to the local base level change induced by the last rupture.

6.2. Excavation Strategy

[21] To constrain the age of scarp formation and to determine the offset across the fault, we cut across the scarp just east of the canyon where Hf3 deposits abut it (Figure 7a). Along this portion of the scarp, its height increases from <2 m to 4.6 m from west to east, due to progressively thinner accumulation of overlapping Hf3 deposits (Figure 8). The north-south excavation was centered midway between the thickest and thinnest accumulation of Hf3 deposits. At this position, the depth of excavation required to observe a significant thickness of hanging wall Hf2 and colluvial deposits is minimized, while the thickness of Hf3 deposits overlapping the fault is maximized.

[22] Overall the excavation was up to 12 m wide, 35 m long, and 9 m deep (Figure 7b). Because of this substantial depth, we benched the west side. This benching exposed three subvertical, overlapping cross sections with 1 to 3 m of horizontal separation (Figures 7c and 9). We will refer to these sections as the upper, middle, and lower walls. On each of these walls, we flagged all important contacts, faults and sample locations using colored nails (e.g., Figure 7b). Then, we determined the relative positions of all nails using a Laser Range Finder, and plotted the positions onto a vertical plane oriented parallel to the excavated walls (171°). These logs were then used as a base for detailed mapping of all contacts and faults

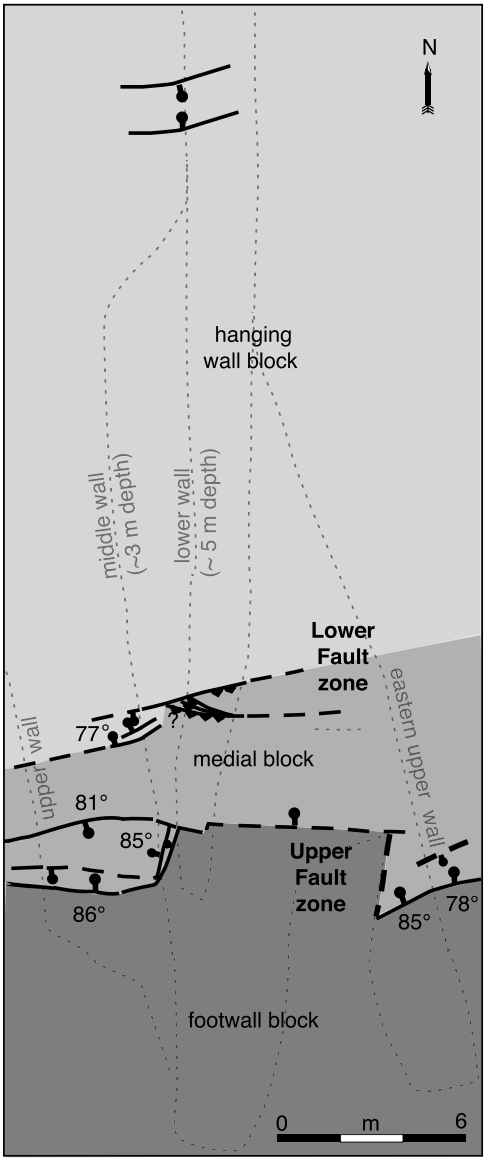

Figure 9. Tectonic map of excavation at Fourmile Canyon showing traces of the upper and lower fault zones projected to a horizontal plane ~5 m below the Hf2 hanging wall surface (ball and bar are on downthrown side of normal faults; teeth are on upthrown side of reverse faults). Also shown are boundaries between vertical and horizontal surfaces in the excavation (thin dashed lines), and the positions of the upper, middle and lower walls.

(e.g., Figures 13a and 13b, and auxiliary file Supp3.eps[1]). To assure continuity among contacts and faults across all three walls, we produced a summary log again using the Laser Range Finder (Figure 10; see auxiliary file Supp2.eps[1] for additional details).

[23] The excavation showed that the surface scarp is underlain by two separate, relatively complex zones of faulting spaced about 4 to 6 m apart. We will refer to the three blocks defined by the faults as the footwall, medial, and hanging wall blocks (Figure 9). The excavation strategy was successful in that the three walls collectively expose a total thickness of 7 m of Hf2 deposits, including a distinctive, ~3 m thick tripartite sequence at the top that is preserved in all three fault blocks, yielding a net vertical displacement across both fault zones of ~5 m (Figure 10 and auxiliary file Supp2.eps[1]). In addition, a thickness of up to 2 m of Hf3 deposits overlaps and preserves colluvial wedge materials that overlap both fault zones.

6.3. Stratigraphy of Excavated Deposits

[24] We have subdivided the excavated section into stratigraphic units 1 to 8, from youngest to oldest, respectively (Figure 11). Unit 1 represents the alluvial fill sequence below surface Hf3; unit 2 represents a paleosol overlying the colluvial deposits of unit 3, which are associated with faulting; and units 4 to 8 represent the alluvial fill sequence below surface Hf2. Detailed lithologic descriptions of each unit (including several subunits) may be found in the auxiliary material[1] (see file Supp4.eps[1]).

[25] The Ht2/Hf2 deposit, units 4 to 8, consists mainly of alluvial gravel intercalated with gravel-rich silt layers and lenses. The gravel layers exhibit contrasts in grain size, degree of sorting, clast versus matrix support, and the development of stratification. The lower unit (8) consists of largely matrix-supported, well-stratified, gravel deposits, with both discontinuous lenses of silt-rich gravel and well-sorted, clast-supported gravel (Figure 12a). Unit 7 has an erosive base into unit 8, and comprises interstratified, clast-supported granular sands and gravel near the base, with the remainder of the unit including more massive, matrix-poor gravel with discontinuous pods and lenses of silt- and carbonate-rich gravel. Unit 6 has an erosive base into unit 7, with discontinuously preserved lenses of clast-supported cobbley gravel. The bulk of the unit consists of well-stratified, clast-supported pebble gravel and granular sand, contrasting with the more massive texture of units above and below (Figure 12b). Unit 5 is a massive matrix-supported gravel with clasts up to cobble size (Figure 12c), which appears to represent a single debris flow about 50 cm thick. It is in gradational contact below a thin deposit of well-stratified, clast-supported gravel of unit 4b. Unit 4a is a silt- and carbonate-rich A_v horizon forming the soil on top of surface Hf2. This A_v horizon is only developed on the footwall block where the Hf2 surface has been exposed to weathering over the last ~2500 yr (Figure 11). On the hanging wall block, where Hf2 was buried beneath colluvial deposits (unit 3), there is no development of an A_v horizon, although there is some enrichment in carbonate-rich silt.

[26] Unit 3 consists of colluvial gravel, sand, and silt with a complex depositional geometry (Figures 10 and 13a). The lower part occurs mainly as fissure fill near the upper fault, and includes massive, poorly sorted silt- and sand-rich gravel with cobbles and boulders of older units, giving way upward to well-stratified, fining-upward cobbley to granular gravel horizons. The middle part consists of well-

[1] Auxiliary material is available at ftp://ftp.agu.org/apend/tc/2003TC001528.

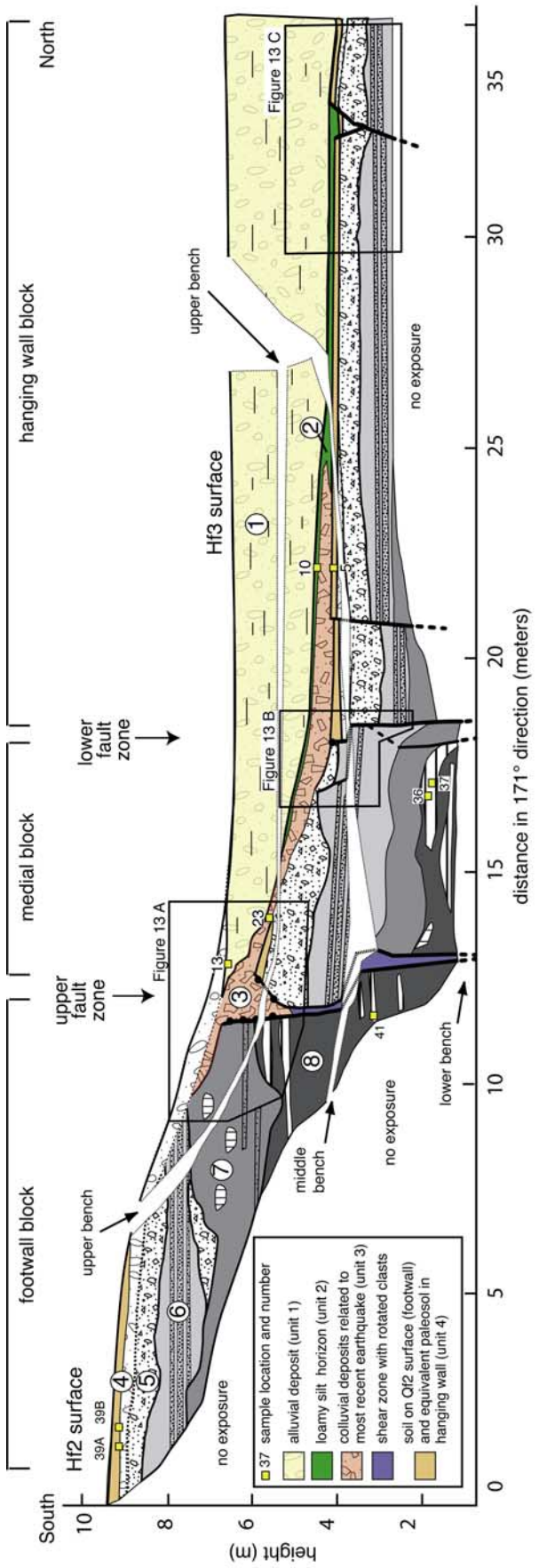

Figure 10. Summary cross section of detailed trench logs looking west, showing fault displacement. Symbols and unit designations are shown in Figure 11. Fault trace, thick lines; free face, line with circles; exposure limit is marked by thin dotted line; numbers show locations of radiocarbon charcoal samples. Detailed trench logs may be found in the auxiliary material.

sorted, clast-supported cobbley gravel with imbrication suggesting down-slope transport. This unit is restricted to the upper part of the medial block. The upper part of unit 3 consists of poorly sorted, matrix-supported, relatively massive gravel distributed across the traces of both faults. The lower and middle parts of unit 3 correspond well to the ''debris-element'' facies association (wedge-shaped deposits resulting primarily by degradation of the free face), and the upper part, to the ''wash-element'' facies association (a relatively surface-parallel mantle formed primarily after the erosion and burial of the free face [*Nelson*, 1992]; see Figure 13a).

[27] Unit 2 (Figure 11) is a thin sandy loam deposited on the medial and footwall blocks. On the medial block, it rests on unit 3. As unit 3 thins northward onto the hanging wall, unit 2 laps onto a substrate of unit 4, and interfingers laterally with the basal deposits of unit 1. The thickness of unit 2 is greatest above small grabens developed in the hanging wall surface (e.g., Figure 13c).

[28] Unit 1 consists of a northward thickening wedge of granular to pebbly, well-sorted, well-stratified clast-supported gravel. Its lower surface onlaps southward onto unit 2, to a position in the middle of the medial block. Along the upper part of the medial block, unit 1 laterally interfingers with the still-active wash element of unit 3. The top of unit 1 has a relatively thin soil horizon that grades laterally up the scarp into a thicker and older soil horizon developed on eroded units 4 through 6 in the footwall (Figure 10).

6.4. Structural Geology

[29] The continuity of units 4 through 6 across all three fault blocks, without significant variations in thickness or facies, strongly suggests that both the upper and lower faults ruptured Hf2 deposits after deposition of unit 4. The continuity of deposition, and the lack of erosion associated with units 4 through 8 in the footwall block, where they are cut by the upper fault indicates that at least the upper fault had no history of motion from unit 8 to unit 4 time.

[30] The net vertical displacement of units 4 through 6 across both faults is measured by projecting unit 4a in the footwall out over the same unit in the hanging wall. This method yields 4.6 ± 0.4 m, including ~3 m on the upper fault and ~1.5 m on the lower fault (Figure 10). Strata in the medial block dip shallowly northeastward, and hence the partitioning of displacement between the two faults varies somewhat along strike.

[31] In detail the geometry of both fault zones is complex. The upper fault is subvertical to steeply north dipping along its excavated trace, with abrupt lateral changes in strike, and 1 to 2 steep antithetic faults developed within the medial block (Figures 9, 10 and 13a). The lower fault dips steeply southward where exposed in the middle and upper sections, and is subvertical in the lower section. It, too, however, accommodates north-side-down motion (Figures 10 and 13b).

[32] Despite the complex fault geometry, the relationships between faulting, fissure fill, and erosion of both the footwall and medial blocks are relatively straightforward. For the lower fault, there is no evidence of a debris element facies association. It appears that the wash element facies association cuts unconformably across the faults. The wash element facies association of unit 3 lies concordantly on unit 4 in the hanging wall block, and cuts across the faults and an erosion surface cut on unit 5 in the medial block (Figures 13a and 13b, and auxiliary file Supp3.eps[1]).

[33] Within the medial block the erosion surface cut on unit 5 gradually rises through units 5 and 4, and the upper debris element facies association pinches in between the wash element and unit 4. The southernmost part of the medial block contains a concordant succession of unit 4 at the position of the Hf2 surface, upper debris element facies association of unit 3, and the wash element facies association of unit 3. The lower debris element facies association fills the graben bounded by the upper fault and its antithetic splay. Portions of the debris element facies association lie in contact with free faces of both the upper fault and its antithetic splay, and exhibit no clast alignment or other evidence of faulting along the contact, in contrast to well developed clast alignment along both faults where they juxtapose pre-Hf2 surface units. We therefore interpret the entire debris element facies association to buttress unconformably against the free faces cut on units 4 and 5 by the upper fault and its antithetic splay.

[34] In the footwall block, the wash element facies association once again lies on deeply eroded pre-Hf2 units, ranging from unit 7 just above the free face of the upper fault up to unit 4 some 6 m to the south of the trace. Here the footwall is capped by the soil horizon defining the Hf2 surface.

[35] At the northernmost end of the trench, units 5, 4, 2, and 1 form a concordant succession with unit 3 absent (Figures 10 and 13c). Here, two small faults and associated fractures form a small graben <10 cm deep. The faults cut units 5 and 4, and are overlapped by units 2 and 1, with unit 2 thickening slightly in association with the graben. Thus, for a distance of 15 m north of the lower fault, and at least 12 m south of the upper fault, units 5, 4, and the Hf2 surface have not been disturbed.

[36] In summary, the last rupture recorded at the Fourmile excavation occurred after fan aggradation to the level of the Hf2 surface, i.e., unit 4a, but prior to deposition of the overlying colluvial deposits of unit 3. On the basis of these relationships we define the event horizon representing the time of last movement on the Crescent fault as the surface between units 4a and 3 in the medial block.

6.5. Geochronology

[37] To determine the age of the event horizon, we collected charcoal from an in situ fire ring and detrital charcoal and charred wood fragments from several stratigraphic levels (Figures 10 and 11). In general, the ^{14}C age of a sample represents the time at which the organic material died. Therefore detrital charcoal grains may yield ^{14}C ages significantly older than their time of deposition. Even ^{14}C ages of charcoal from the fire ring may thus overestimate its in situ age.

[38] In the Fourmile excavation, charcoal generally occurs throughout the exposed section as detrital fragments

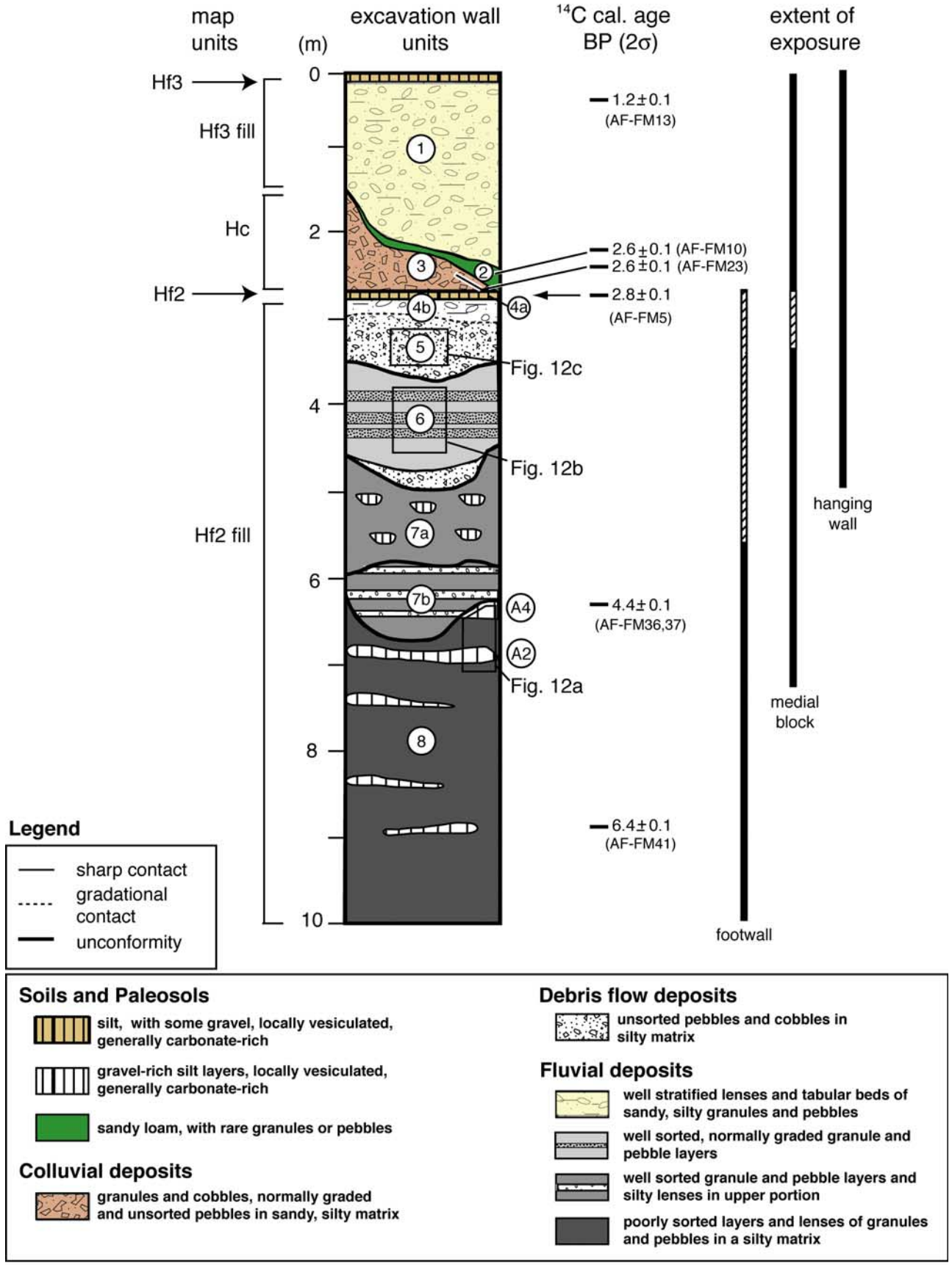
map units
(m)
excavation wall units
14C cal. age BP (2σ)
extent of exposure
Hf3
Hf3 fill
Hc
Hf2
Hf2 fill
0
2
4
6
8
10
1
2
3
4a
4b
5
6
7a
7b
8
A4
A2
1.2±0.1 (AF-FM13)
2.6±0.1 (AF-FM10)
2.6±0.1 (AF-FM23)
2.8±0.1 (AF-FM5)
4.4±0.1 (AF-FM36,37)
6.4±0.1 (AF-FM41)
Fig. 12c
Fig. 12b
Fig. 12a
hanging wall
medial block
footwall
Legend
sharp contact
gradational contact
unconformity
Soils and Paleosols
silt, with some gravel, locally vesiculated, generally carbonate-rich
gravel-rich silt layers, locally vesiculated, generally carbonate-rich
sandy loam, with rare granules or pebbles
Colluvial deposits
granules and cobbles, normally graded and unsorted pebbles in sandy, silty matrix
Debris flow deposits
unsorted pebbles and cobbles in silty matrix
Fluvial deposits
well stratified lenses and tabular beds of sandy, silty granules and pebbles
well sorted, normally graded granule and pebble layers
well sorted granule and pebble layers and silty lenses in upper portion
poorly sorted layers and lenses of granules and pebbles in a silty matrix

Figure 11.

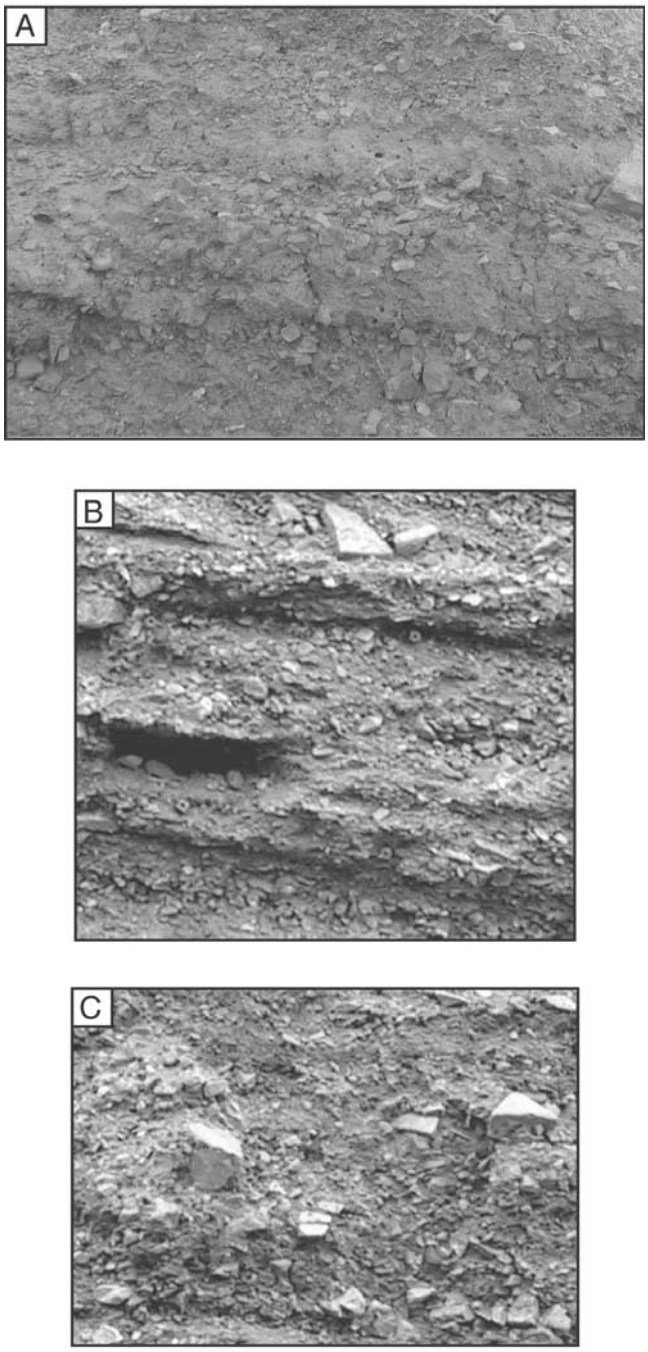

Figure 12. Photographs of typical strata. (a) Silt-supported gravel layers with lenses of discontinuous sandy clast-supported gravel stringers typical of unit 8; (b) clast-supported, pebbly sheet flood couplets characteristic of unit 6; and (c) matrix-supported, cobbley debris flow of unit 5.

and is particularly abundant in silt-rich layers. The two lowest samples are from silt-rich layers in unit 8, each of which has abundant charcoal, and the four uppermost samples are from units 1, 2, 3 and 4. Unit 8 samples represent deposition from a source terrain rich in charcoal. Because the preservation of abundant charcoal after a fire is relatively brief, we presume burning, death, and deposition occurred over a time period of a few years to a few decades. In contrast, the four stratigraphically higher samples were sparse, isolated grains, and therefore could be significantly older than the time of deposition of their host gravels. The remaining charcoal sample was collected from an anthropogenic fire ring in unit 4a (sample AFFM-05, Figure 10).

[39] Charcoal sample preparation and determination of isotopic ratios for ^{14}C analysis using an accelerator mass spectrometer followed standard protocols [*Stuiver et al.*, 1998a, 1998b; *Trumbore*, 2000]. We report all ^{14}C ages in calibrated calendar years before present (BP; present is defined as the year 1950) with their 2σ errors, based on the calibration by tree ring record of *Stuiver et al.* [1998b] (Table 1 and Appendix A).

[40] Radiocarbon ages from the Fourmile charcoal samples correlate well with their stratigraphic position, with the exception of sample AFFM-39, which at 10.6 ± 0.1 ka is much older than all of the other samples and is therefore older than deposition of the exposed section. The other ages increase in linear proportion with stratigraphic depth, ranging from 1.3 ± 0.1 ka at the gradational contact between units 1 and 3 to 6.4 ± 0.1 ka near the base of unit 8, and indicate an average sedimentation rate of ~1.8 mm/yr (Figure 14). The apparent uniform sedimentation rate defined by the age data including sample AFFM-05 from the fire ring suggests that none of the detrital samples significantly predate the time of their deposition.

[41] The age of the event horizon is best constrained by the sample AF5 from the fire ring which yields an age of 2.8 ± 0.1 ka B.P. (Table 1 and Appendix A). The fire pit was built on the Hf2 surface, but its precise relationship to the time of soil development represented by unit 4a is not well defined. Hence the 2.8 ka age determination represents a minimum age of deposition of unit 4b gravel. The maximum age of the Hf2 surface is 4.4 ± 0.1 ka, the age of the youngest sample below unit 4b, at the top of unit 8. Because there are at least five independent depositional events between the top of unit 8 and unit 4a (units 7b, 7a, 6, 5, and 4b; Figure 11), and the overall character of deposition appears to be uniform in time from 6 ka to 1 ka, the age of unit 4b is much closer to 2.8 ka than to 4.4 ka. The lack of development of a significant unit 4a soil in the hanging wall, as noted earlier, also suggests that there was relatively little time between deposition unit 4b and unit 3.

Figure 11. Stratigraphic column of sedimentary deposits in the Fourmile Canyon excavation used to determine the stratigraphic depths of radiocarbon samples. Numbers in circles indicate units described in text. Stratigraphic positions of Hf3, Hf2, their fill sequences and the colluvial wedge appear on left. The range of exposure of the section in each structural block appears on the right. The hatched pattern indicates strata that were eroded following the rupture in the footwall adjacent to each fault. The stratigraphic column was constructed based on correlation of marker units across the three blocks. More detailed descriptions of stratigraphic units are in auxiliary file Supp4.eps.

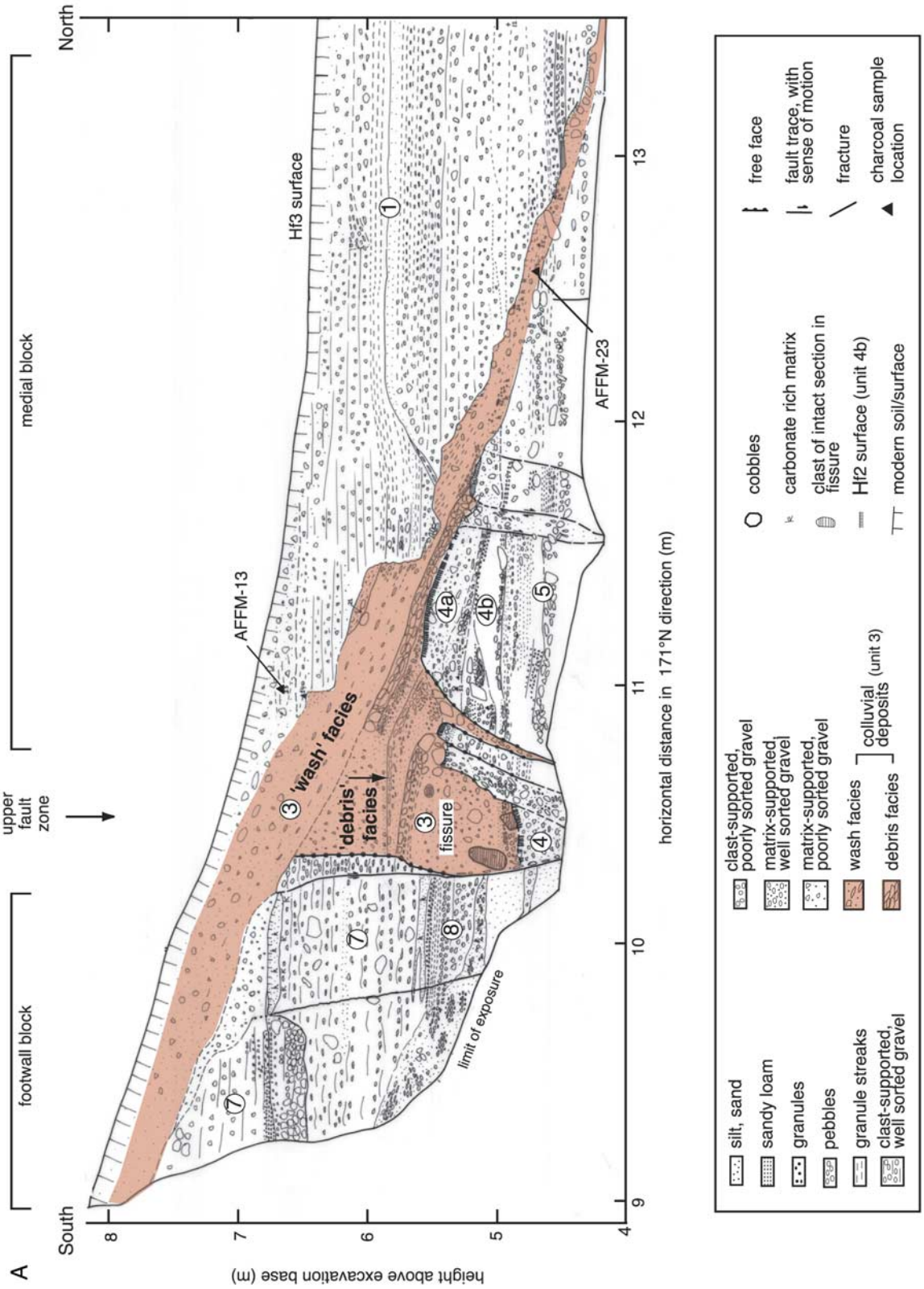

Figure 13. (a) Detail of upper wall trench log, showing interaction between upper fault zone, colluvial deposits and Hf3 fill sequence. (b) Photograph and detailed interpretation of the middle wall showing the lower fault zone and its interaction with colluvial deposits (unit 3) and the fill sequence of Hf3 (unit 1). (c) Detail of the northernmost portion of the middle wall showing the relationships between the event horizon, faulted unit 4 deposits and unfaulted unit 2 deposits.

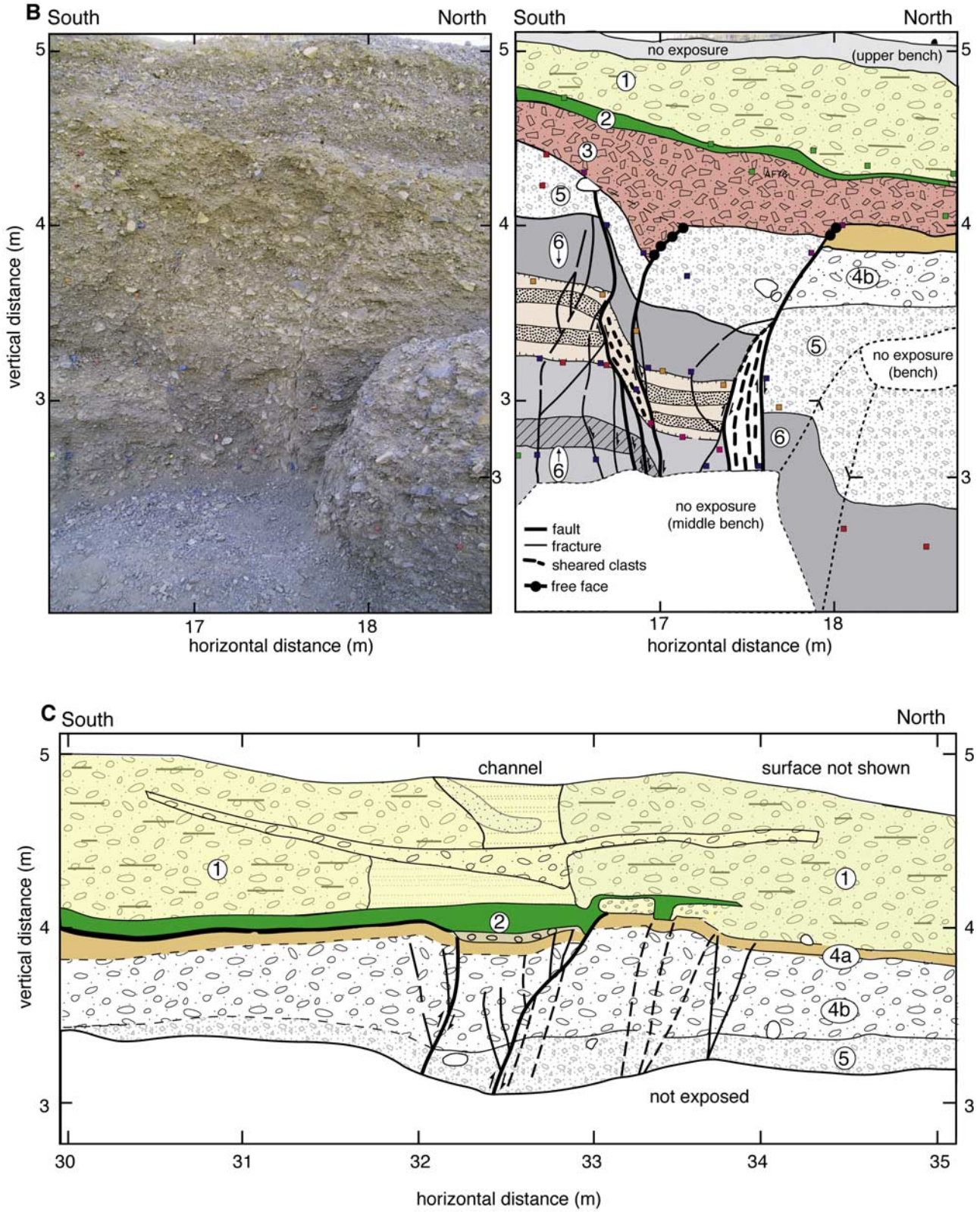

Figure 13. (continued)

Table 1. Accelerator Mass Spectrometer Radiocarbon Age Estimates on Charcoal From the Fourmile Excavation, Crescent Valley, Nevada

Sample No.[a]	Measured Radio Carbon Age,[b] years	$\delta^{13}C$,[c] ‰	Conventional ^{14}C,[d] years B.P.	Calibrated Age,[e] (calendar years B.P.) 2σ	Average, cal years B.P. (2σ)[f]	Combined Average, 2σ cal years B.P. (Conservative Estimate)[g]	Sample Description (in Stratigraphic Order)
AFFM-13	1320 ± 40	−24.7	1320 ± 40	1300 to 1170	1235 ± 65	1235 ± 65	charcoal from upper portion of fluvial gravel of Hf3, provides maximum age of Hf3 surface
AFFM-10	2510 ± 40	−23.2	2540 ± 40	2750 to 2690 and 2660 to 2480	2720 ± 30 2570 ± 90	2645 (+105 −165)	charcoal in sandy loam of unit 2, provides maximum age of unit 2
AFFM-23	2590 ± 50	−24.1	2600 ± 50	2780 to 2710 and 2560 to 2540	2745 ± 35 2550 ± 10	2648 (+132 −108)	charcoal from colluvial wedge, unit 3, provides maximum age of unit 3
AFFM-05	2630 ± 40	−22.6	2670 ± 40	2850 to 2740	2795 ± 55	2795 ± 55	charcoal from fire ring in buried Hf2 surface, hanging wall, approximates event age
AFFM-39	9410 ± 40	−29.4	9340 ± 40	10660 to 10430	10545 ± 115	10545 ± 115	charred material from below the Qf2 surface in footwall, sample is assumed to have had an inherited age at the time of deposition
AFFM-36+37	3950 ± 40	−23.9	3970 ± 40	4520 to 4350 and 4330 to 4300	4435 ± 115 4315 ± 15	4375 (+145 −75)	charcoal from clay-rich silt of unit 8A4, provides a minimum date of penultimate event
AFFM-41	5650 ± 40	−25.8	5640 ± 40	6490 to 6320	6405 ± 85	6405 ± 85	charcoal from silty layer (unit 8), footwall, provides minimum age of penultimate event

[a]See trench logs Figures 11 and 13a and auxiliary files Suppl 2 and Supp3 (detailed trench logs) for precise sample locations.

[b]Charcoal samples with a weight of 1 to 5 mg were prepared and analyzed by BETA Analytic, Inc., 4985 SW 74 Court, Miami, Florida 33155, USA, following their standard treatment procedure. Sample preparation included crushing of the charcoal material, cleaning of the sample with hot alkali and acids to remove contaminants, associated sediments and rootlets. The sample is then reduced to graphite (100% carbon) for analysis in an accelerator mass spectrometer. Raw age measurements are reported based on the Libby ^{14}C half life (5568 years).

[c]Measured $^{13}C/^{12}C$ isotopic ratios are calculated relative to the PDB-1 international standard.

[d]Measured radiocarbon age has been corrected for $^{13}C/^{12}C$ fractionation to obtain the conventional radiocarbon age, i.e., the age is normalized to −25 per mil $\delta^{13}C$.

[e]To obtain the calibrated age, the conventional radiocarbon age in ^{14}C years has been calibrated against calendar years (in years before present, which is before 1950) based on comparing the conventional age to a spline fit through the tree ring calibration of *Stuiver et al.* [1998a, 1998b]; *Stuiver and van der Plicht* [1998]; and *Talma and Vogel* [1993].

[f]Average of the age range from the calibrated age curve with 2σ uncertainties.

[g]In cases of two intersections of the conventional age with the tree ring calibration curve, a conservative age has been calculated by averaging the two ages, assuming equal probability for the two age bins.

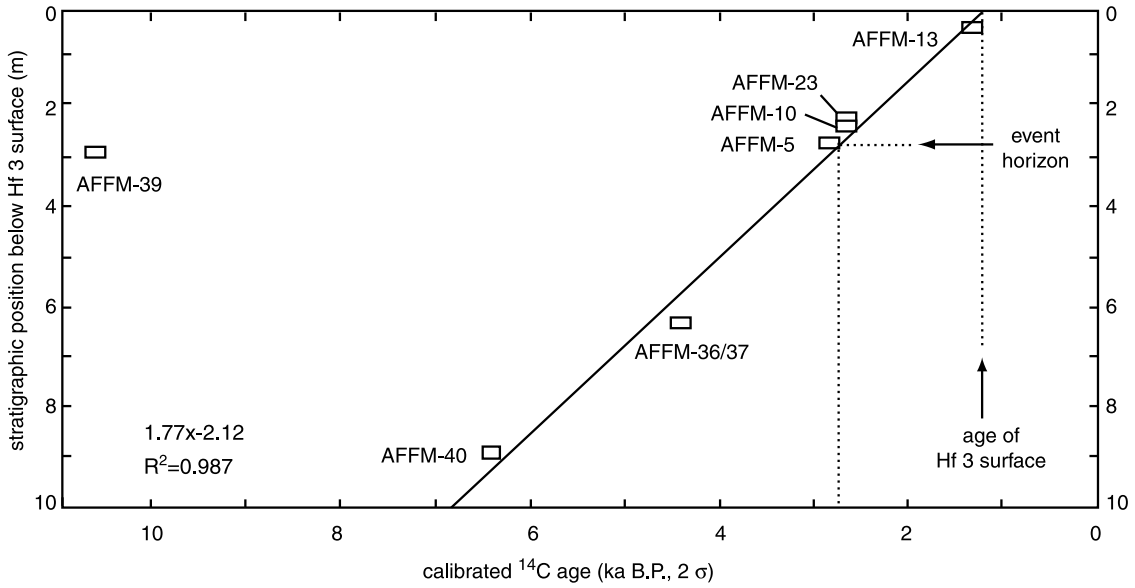

Figure 14. Graph of stratigraphic position versus age of charcoal samples. The Hf3 surface is defined at an elevation of zero meters. Depth estimates of the charcoal samples from the medial and footwall blocks have been determined based on their location in the stratigraphic column (Figure 11). The sizes of the boxes represent uncertainties in age (Table 1) and depth (Figure 11).

[42] A brief exposure interval of the hanging wall Hf2 surface is also supported by the fact that overlying deposits of units 3 and 2 are about the same age as the fire pit. The maximum age of detrital charcoal fragment AFFM-23 from the lower wash facies element association of unit 3 is 2.75 ± 0.04 ka B.P, with an average age of 2.6 ± 0.1 ka B.P. (Appendix A and Table 1). Charcoal fragment AFFM-10, which occurs in the sandy loam of unit 2, just 10 cm above the fire pit, also yields an average age of 2.6 ± 0.1 ka. If hanging wall Hf2 had been exposed for any significant fraction of the interval 4.4 to 2.8 ka (i.e., deposition of units 7b to 4b was complete substantially prior to 2.8 ka), it would be coincidental that the fire pit was built on the surface within 100 to 200 years prior to deposition of unit 3.

[43] In summary, the apparent uniformity of deposition rate, the relatively large number of independent depositional events, the lack of soil development in hanging wall unit 4a, and the similarity in ages immediately above and below the colluvial wedge, all suggest the age of the event horizon is ~2.8 ± 0.1 ka to 2.6 ± 0.1 ka.

7. Discussion

[44] The measured offsets of Hf2 along the range front appear to define a slip function that is typical of historic Basin and Range earthquakes. Slip rates in the 0.3 mm/yr range for a typical Basin and Range fault, assuming 3 m per event, implies recurrence intervals of order 10^4 yrs. The fact that surface Hf2 is only ca. 2.8 kyr old, a relatively small fraction of this value, supports the hypothesis that the measured offsets along the trace (Figure 6b) probably occurred during a single late Holocene earthquake. Comparison of the net vertical tectonic displacement of 4.2 m estimated prior to excavation, versus the measured 4.6 ± 0.4 m, suggests many of the other estimates along the range front may also be slightly lower than the actual net vertical tectonic displacement because of postseismic aggradation on the hanging wall block. If we assume a 55° dipping fault plane, a minimum rupture length of 30 km (the minimum extent of measured offset Hf2 surfaces on Figure 5), fault slip extending to 15 km depth, an average of 5 m of dip slip (assuming >4 m NVTD along most of the trace) and an elastic modulus of 3×10^{10} Nm^{-2}, the moment magnitude of the event was at least $M_w = 7.3$. Using a large empirical database, *Wells and Coppersmith* [1994] developed a set of equations that relate M_w to rupture length, rupture area, average displacement, and maximum displacement. Using these equations for a rupture length of 30 km, average surface offset of 5.0 m, and maximum surface offset of 7 m yields an estimated M_w that ranges from 6.6 to 7.3.

[45] If earthquakes along the Crescent fault were typically of this size, we can estimate the average recurrence interval on the basis of: (1) the total vertical displacement along the range front since 14 Ma (assuming uniform behavior), (2) known Holocene to late Quaternary vertical offset rates on Basin and Range normal faults (assuming uniformity among Basin and Range faults), or (3) the average horizontal strain accumulation rate in the Basin and Range determined geodetically. Given 3 km of vertical displacement since 14 Ma, the average vertical rate is 0.2 mm/yr. Based on a compilation of geologic vertical displacement rates of faults from the eastern Great Basin, *Niemi et al.* [2004] and *Friedrich et al.* [2003] determined that typical late Quaternary vertical rates lie between 0.2 and 0.4 mm/yr (Figure 15). Given the average horizontal extensional strain rate across the Basin and Range at present (excluding of

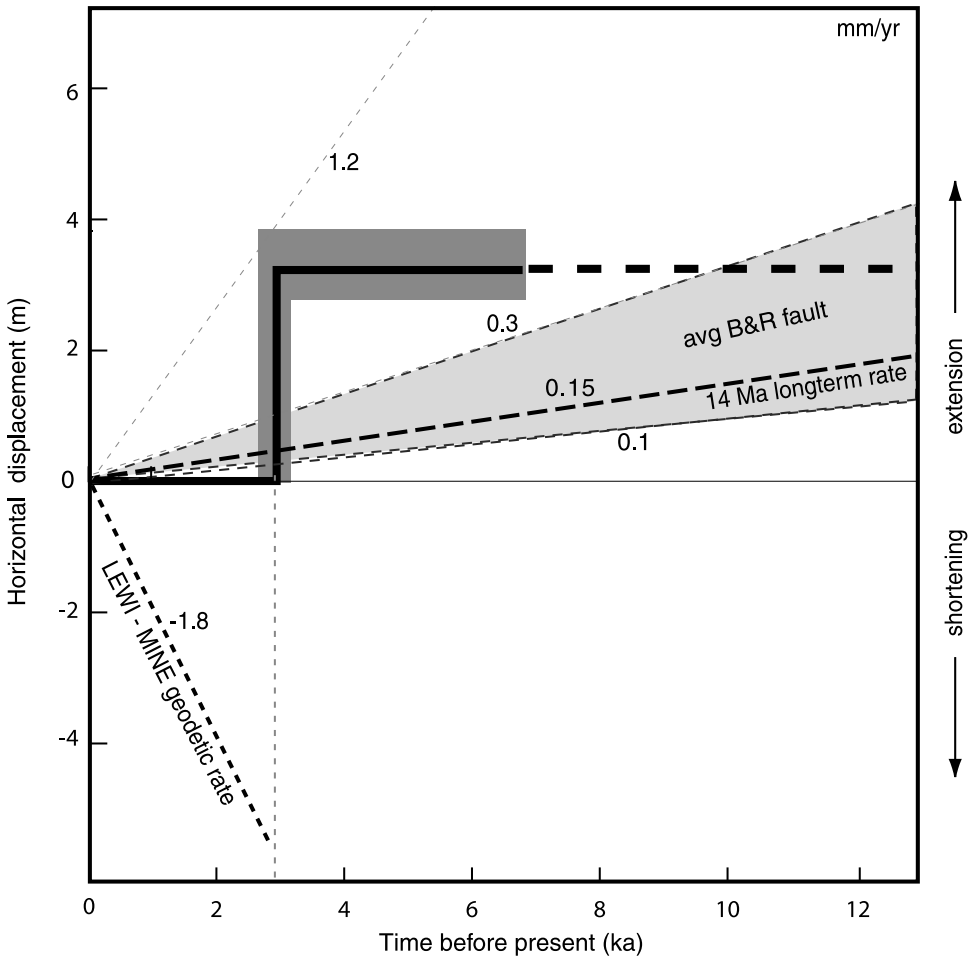

Figure 15. Graph showing comparison of horizontal displacement versus time across the Crescent fault based on geodetic and paleoseimic data. We assume (1) that most of the velocity between LEWI and MINE reflects motion along the Crescent fault, and (2) a 55° dip of the fault through the seismogenic crust (thick curve, gray shading showing uncertainties) Range of typical late Quaternary horizontal Basin and Range rates (gray); 14 Ma long-term rate for the Crescent fault (thick dash).

course the baseline LEWI - MINE) of 10 nstr/yr, a typical 30-km-wide range block accumulates horizontal strain at about 0.3 mm/yr. Therefore, assuming 3 to 4 m of either vertical or horizontal displacement for each event, we estimate an average recurrence interval of 10,000 to 12,500 years for the Crescent fault. Because we observe only the most recent event at ~2.8 ka and an absence of faulting back to ~6.4 ka, we cannot distinguish whether or not strain release on the fault is clustered, as appears to be the case for the Wasatch fault zone, Utah [e.g., *Machette et al.*, 1992a, 1992b; *McCalpin and Nishenko*, 1996; *Friedrich et al.*, 2003].

[46] The occurrence of a late Holocene earthquake on the Crescent fault, in addition to being at odds with the contemporary shortening across the baseline LEWI-MINE, limits the timescale over which shortening has taken place (Figure 15). Shortening normal to the range front would serve to reduce stress on the Crescent fault. Presumably, the time period leading up to the most recent event at 2.8 ka was characterized by at least a few millennia wherein the average geodetic displacement rate was extensional normal to the fault trace. Therefore transient shortening could not have persisted in the area for more than the last 2.8 kyr. Of course, this transient could have a duration anywhere between the decadal timescale of geodetic observation and the millennial timescale of geologic deformation.

8. Conclusions

[47] The overarching lesson to be drawn from our characterization of the Crescent fault is that despite the fact that the fault is nearly three millennia into its postseismic interval (~25% of its estimated mean recurrence interval) the contemporary strain is unambiguously transient. As argued by *Wernicke et al.* [2000], the shortening across LEWI-MINE is plausibly the result of postseismic viscoelastic relaxation from historic Basin and Range earthquakes some 100 km to the west of Crescent Valley, namely the 1915 Pleasant Valley and 1954 Rainbow

Mountain-Dixie Valley-Fairview Peak earthquake sequence [*Wallace*, 1977; *Caskey et al.*, 1996]. However, more recent geodetic solutions of the Basin and Range suggest that shortening may occur in places that are not easily explained by models of postseismic viscoelastic relaxation [*Bennett et al.*, 2003]. Regardless of the cause of this transient, the situation in Crescent Valley indicates that differences between local geodetic velocities and velocities estimated from geologic data may be expected, up to the level of contrasting sign.

Apendix A: ^{14}C Sample Descriptions

[48] We analyzed four samples below the event horizon. The stratigraphically lowest sample, AF-FM-41, is a small charcoal fragment from a silty layer within unit 8, exposed in the footwall near the base of the excavation. This sample yields a conventional radiocarbon age of 5.64 ± 0.04 kyr that corresponds to a calibrated calendar age of 6.40 ± 0.09 ka. The next higher sample, AF-FM-3637, consists of small charcoal fragments from a charcoal-rich gravelly silt layer of the medial block (Figure 10), and yields a conventional radiocarbon age of 3.95 ± 0.04 kyr, giving two intersections with the tree ring calibration curve of *Stuiver* [1998a], 4.44 ± 0.12 ka and 4.31 ± 0.02 ka. In the footwall, several centimeters below the Hf2 surface, a charred horizon is exposed, which consists of purple to black, carbon-stained soil and a few very small dispersed charcoal fragments (sample AF-FM-39). The conventional ^{14}C age of this sample is 9.34 ± 0.04 kyr, resulting in a calibrated calendar age of 10.55 ± 0.12 ka. Charcoal sample AF-FM-05 has been picked from a ~20 cm long in situ fire pit just below the surface Hf2 in the hanging wall (Figure 10). The conventional age for this sample is 2.67 ± 0.04 kyr, corresponding to a calibrated calendar age of 2.80 ± 0.06 ka.

[49] We analyzed three charcoal samples from localities above the event horizon. The lower two of these samples were derived from within the colluvial wedge and directly above it in unit 2. Sample AF-FM-23 was a blocky charcoal fragment in the lower portion of the wash element facies association in the upper section of the medial block. The conventional age of this sample is 2.60 ± 0.05 yrs, which results in two intersections of the tree ring calibration curve at 2.75 ± 0.04 and 2.55 ± 0.01 years, respectively. Sample AF-FM-10 consists of several small charcoal fragments that occurred within the sandy loam of unit 2, a few centimeters above the firepit in the middle section of the hanging wall. This sample yields a conventional ^{14}C age of 2.54 ± 0.04 yrs, which corresponds to 2.72 ± 0.03 and 2.57 ± 0.09 yrs on the tree ring calibration curve. The highest sample, AF-FM-13, was found in the southernmost exposure of unit 1, where it interfingers with colluvial deposits from the scarp. The conventional age of this sample is 1.32 ± 0.04 yrs, which corresponds to a calibrated calendar age of 1.24 ± 0.07 yrs.

[50] **Acknowledgments.** This study was supported by NSF grants EAR 99-03366 and EAR-00-01209 awarded to B. Wernicke and K. Sieh, and grant EAR-9902968 awarded to J. Lee. A. Friedrich acknowledges additional financial support from the University of Potsdam. We thank M. Jackson and R. Bruhn for providing surveying equipment, and B. Phillibosian, R. Heermance, and J. Liu for valuable assistance in the field. We benefited from reviews by D. Hindle, S. Mc Gill, and R. Hetzel and discussions with J. Bell, J. Caskey, C. DePolo, K. Haller, M. Machette, A. Ramelli, and S. Wesnousky on Basin and Range paleoseismology.

References

Arabasz, W. J., R. B. Smith, W. D. Richins, E. R. Anderson, and A. S. Ryall (1980), Earthquake studies along the Wasatch Front, Utah: Network monitoring, seismicity, and seismic hazards, *Bull. Seismol. Soc. Am.*, *70*, 1479–1499.

Beanland, S., G. H. Blick, and D. J. Darby (1990), Normal faulting in a back-arc basin: Geological and geodetic characteristics of the 1987 Edgecumb earthquake, New Zealand, *J. Geophys. Res.*, *95*, 4693–4707.

Bell, J. W., C. M. DePolo, A. R. Ramelli, A. M. Sarna-Wojcicki, and C. E. Meyer (1999), Surface faulting and paleoseismic history of the 1932 Cedar Mountain earthquake area, west-central Nevada and implications for modern tectonics of the Walker Lane, *Geol. Soc. Am. Bull.*, *111*, 791–807.

Bennett, R. A., J. L. Davis, and B. P. Wernicke (1999), Present-day pattern of Cordilleran deformation in the Western United States, *Geology*, *27*, 371–374.

Bennett, R. A., B. P. Wernicke, N. A. Niemi, A. M. Friedrich, and J. L. Davis (2003), Contemporary strain rates in the northern Basin and Range province from GPS data, *Tectonics*, *22*(2), 1008, doi:10.1029/2001TC001355.

Bucknam, R. C., and R. E. Anderson (1979), Estimation of fault-scarp ages from a scarp-height-slope-angle relationship, *Geology*, *7*, 11–14.

Caskey, S. J., S. G. Wesnousky, Z. Peizhen, and D. B. Slemmons (1996), Surface faulting of the 1954 Fairview Peak (M_s 7.2) and Dixie Valley (M_s 6.8) earthquakes, central Nevada, *Bull. Seismol. Soc. Am.*, *86*, 761–787.

Crone, A., M. Machette, M. G. Bonilla, J. J. Lienkaemper, K. L. Pierce, W. E. Scott, and R. C. Bucknam (1987), Surface faulting accompanying the Borah Peak earthquake and segmentation of the Lost River fault, central Idaho, *Bull. Seismol. Soc. Am.*, *77*, 739–770.

Davis, J. L., R. A. Bennett, and B. P. Wernicke (2003), Assessment of GPS velocity accuracy for the Basin and Range Geodetic Network (BARGEN), *Geophys. Res. Lett.*, *30*(7), 1411, doi:10.1029/2003GL016961.

DeMets, C., R. G. Gordon, D. F. Argus, and S. Stein (1994), Effect of recent revisions to the geomagnetic reversal timescale on estimates of current plate motions, *Geophys. Res. Lett.*, *21*, 2191–2194.

dePolo, D. M., and C. M. dePolo (1999), Earthquakes in Nevada 1852–1998, *Map 119*, 1:1,000,000 scale, Nev. Bur. of Mines and Geol., Reno.

Dixon, T. H., E. Norabuena, and L. Hotaling (2003), Paleoseismology and Global Positioning System: Earthquake-cycle effects and geodetic versus geologic fault slip rates in the eastern California shear zone, *Geology*, *31*, 55–58.

Dohrenwend, J. C., B. A. Schell, C. M. Menges, B. C. Moring, and M. A. McKittrick (1996), Reconnaissance photogeologic map of young (Quaternary and late Tertiary) faults in Nevada, in *An Analysis of Nevada's Metal-Bearing Mineral Resources*, edited by D. A. Singer, *Nev. Bur. Mines Geol. Open File Rep., 96-2*, plate 9.

Doser, D. I., and R. B. Smith (1982), Seismic moment rates in the Utah region, *Bull. Seismol. Soc. Am.*, *72*, 525–551.

Friedrich, A. M., B. P. Wernicke, N. A. Niemi, R. A. Bennett, and J. L. Davis (2003), Comparison of geodetic and geologic data from the Wasatch region, Utah, and implications for the spectral character of Earth deformation at periods of 10 to 10 million years, *J. Geophys. Res.*, *108*(B4), 2199, doi:10.1029/2001JB000682.

Gilluly, J., and O. Gates (1965), Tectonic and igneous geology of the northern Shoshone Range, Nevada, 153 pp., *U.S. Geol. Surv. Prof. Pap., 465*.

Gilluly, J., and H. Masursky (1965), Geology of the Cortez Quadrangle, Nevada, *U.S. Geol. Surv. Bull., 1175*, 117 pp.

Grant, L. B., and K. Sieh (1994), Paleoseismic evidence of clustered earthquakes on the San Andreas fault in the Carrizo Plain, California, *J. Geophys. Res.*, *99*, 6819–6841.

Hecker, S. (1993), Quaternary tectonics of Utah with emphasis on earthquake-hazard characterization, *Utah Geol. Surv. Bull.*, *127*, 157 pp.

Lee, J., J. Spencer, and L. Owen (2001), Holocene slip rates along the Owens Valley fault, California: Implications for the recent evolution of the eastern California shear zone, *Geology*, *29*, 819–822.

Machette, M. N., S. F. Personius, and A. R. Nelson (1992a), Paleoseismology of the Wasatch fault zone: A summary of recent investigations, interpretations, and conclusions, in *Assessment of Regional Earthquake Hazards and Risk Along the Wasatch Front, Utah*, edited by P. L. Gori and W. W. Hays, *U.S. Geol. Surv. Prof. Pap.*, *1500*, A1–A71.

Machette, M. N., S. F. Personius, A. R. Nelson, R. C. Bucknam, and P. L. Hancock (1992b), The Wasatch fault zone, U.S.A., *Annal. Tectonicae*, *6*, *Suppl.*, 5–39.

Machette, M. N., C. Menges, J. Slate, A. J. Crone, R. E. Klinger, L. A. Piety, A. M. Sarna-Wojcicki, and R. A. Thompson (2001), Field trip guide for day B, Furnace Creek area, in *Quaternary and Late Pliocene Geology of the Death Valley Region: Recent Observations on Tectonics, Stratigraphy, and Lake Cycles, Pacific Cell—Friends of the Pleistocene Field Trip, February 17–19, 2001*, edited by M. N. Machette, M. L. Johnson, and J. L. Slate, *U.S. Geol. Surv. Open File Rep. 01-51*.

McCalpin, J. P., and S. P. Nishenko (1996), Holocene paleoseismicity, temporal clustering, and probabilities of future large ($M > 7$) earthquakes on the Wasatch fault zone, Utah, *J. Geophys. Res.*, *101*, 6233–6253.

McGill, S., and K. Sieh (1993), Holocene slip rate of the central Garlock fault in southeastern Searles Valley, California, *J. Geophys. Res.*, *98*, 14,217–14,231.

Meriaux, A.-S., P. Tapponnier, J. van der Woerd, R. C. Finkel, M. W. Caffee, C. Lasserre, X. Xu, H. Lee, and C. Xu (2000), Fast extrusion of the Tibet plateau: A 3 cm/yr, 100 Kyr slip-rate on the Altyn Tagh fault, *Eos Trans. AGU*, *81*(48), Fall Meet. Suppl., Abstract T62D-07.

Miller, M. M., D. J. Johnson, T. H. Dixon, and R. K. Dokka (2001), Refined kinematics of the eastern California shear zone from GPS observations, 1993–1998, *J. Geophys. Res.*, *106*, 2245–2264.

Myers, W. B., and W. Hamilton (1964), Deformation accompanying the Hebgen Lake earthquake of August 17, 1959, in *The Hebgen Lake, Montana, Earthquake of August 17, 1959*, *U. S. Geol. Surv. Prof. Pap.*, *P 0435*, 55–98.

Nelson, A. R. (1992), Lithofacies analysis of colluvial sediments: An aid in interpreting the Recent history of Quaternary normal faults in the Basin and Range Province, western United States, *J. Sediment. Petrol.*, *62*, 607–621.

Niemi, N. A., B. P. Wernicke, A. M. Friedrich, R. A. Bennett, and J. L. Davis (2004), BARGEN continuous GPS data across the eastern Basin and Range Province and implications for fault system dynamics, *Geophys. J. Int.*, in press.

Peltzer, G., F. Crampe, S. Hensley, and P. Rosen (2001), Transient strain accumulation and fault interaction in the eastern California shear zone, *Geology*, *29*, 975–978.

Reheis, M. (1999), Extent of Pleistocene lakes in the western Great Basin, *U.S. Geol. Surv. Misc. Field Stud. Map, 2323*.

Sella, G. F., T. H. Dixon, and A. L. Mao (2002), REVEL: A model for Recent plate velocities from space geodesy, *J. Geophys. Res.*, *107*(B4), 2081, doi:10.1029/2000JB000033.

Slemmons, D. B. (1957), Geologic effects of the Dixie Valley-Fairview Peak, Nevada, earthquakes of December 16, 1954, *Bull. Seismol. Soc. Am.*, *47*, 353–357.

Smith, R. B., and M. L. Sbar (1974), Contemporary tectonics and seismicity of the western United States with emphasis on the Intermountain Seismic Belt, *Geol. Soc. Am. Bull.*, *85*, 1205–1218.

Stewart, J. H. (1971), Basin and Range structure: A system of horsts and grabens produced by deep-seated extension, *Geol. Soc. Am. Bull.*, *82*, 1019–1043.

Stewart, J. H. (1978), Basin-range structure in western North America: A review, in *Cenozoic Tectonics and Regional Geophysics of the Western Cordillera*, edited by R. B. Smith and G. P. Eaton, *Mem. Geol. Soc. Am.*, *152*, 1–31.

Stuiver, M. and J. van der Plicht (Eds.) (1998), INTCAL98, Calibration Issue, *Radiocarbon*, *40*, 1041–1164.

Stuiver, M., P. J. Reimer, and T. F. Braziunas (1998a), High-precision radiocarbon age calibration for terrestrial and marine samples, *Radiocarbon*, *40*, 1127–1151.

Stuiver, M., P. J. Reimer, E. Bard, J. W. Beck, G. S. Burr, K. A. Hughen, B. Kromer, G. McCormac, J. van der Plicht, and M. Spurk (1998b), INTCAL98 radiocarbon age calibration, 24,000-0 cal BP, *Radiocarbon*, *40*, 1041–1083.

Talma, A. S., and J. C. Vogel (1993), A simplified approach to calibrating (super) ^{14}C dates, *Radiocarbon*, *35*, 317–322.

Thompson, G. A., and D. B. Burke (1973), Rate and direction of spreading in Dixie Valley, Basin and Range Province, Nevada, *Geol. Soc. Am. Bull.*, *2*, 627–632.

Trumbore, S. E. (2000), Radiocarbon geochronology, in *Quaternary Geochronology: Methods and Applications*, *AGU Ref. Shelf Ser.*, vol. 4, edited by J. S. Noller, J. M. Sowers, and W. R. Lettis, pp. 41–60, AGU, Washington. D. C.

Wallace, R. E. (1977), Profiles and ages of young fault scarps, north-central Nevada, *Geol. Soc. Am. Bull.*, *88*, 1267–1281.

Wallace, R. E. (1984a), Eyewitness account of surface faulting during the earthquake of 28 October 1983, Borah Peak, Idaho, *Bull. Seismol. Soc. Am.*, *74*, 1091–1094.

Wallace, R. E. (1984b), Fult scarps formed during the earthquakes of October 2, 1915, in Pleasant Valley, Nevada, and some tectonic implications: Faulting related to the 1915 earthquakes in Pleasant Valley, Nevada, *U.S. Geol. Surv. Prof. Pap.*, A1–A33.

Wang, Q., et al. (2001), Present-day crustal deformation in China constrained by global positioning system measurements, *Science*, *294*, 574–577.

Wells, D. L., and K. J. Coppersmith (1994), New empirical relationships among magnitude, rupture length, rupture width, rupture area, and surface displacement: *Bull. Seismol. Soc. Am.*, *84*, 974–1002.

Wernicke, B., A. M. Friedrich, N. A. Niemi, R. A. Bennett, and J. L. Davis (2000), Dynamics of plate boundary fault systems from Basin and Range Geodetic Network (BARGEN) and geological data, *GSA Today*, *10*, 1–7.

Witkind, I. J., J. B. Hadley, and W. H. Nelson (1964), Pre-Tertiary stratigraphy and structure of the Hebgen Lake area, in *The Hebgen Lake, Montana, Earthquake of August 17, 1959*, *U. S. Geol. Surv. Prof. Pap.*, *P 0435*, 199–207.

Zoback, M. L. (1989), State of stress and modern deformation of the northern Basin and Range Province, *J. Geophys. Res.*, *94*, 7105–7128.

Zoback, M. L., and G. A. Thompson (1978), Basin and range rifting in northern Nevada: Clues from a mid-Miocene rift and its subsequent offsets, *Geology*, *6*, 111–116.

Zoback, M. L., and M. D. Zoback (1980), Faulting patterns in north-central Nevada and strength of the crust, *J. Geophys. Res.*, *85*, 275–284.

Zoback, M. L., E. H. McKee, R. J. Blakely, and G. A. Thompson (1994), The northern Nevada rift: Regional tectono-magmatic relations and middle Miocene stress direction, *Geol. Soc. Am. Bull.*, *106*, 371–382.

A. M. Friedrich, Institute of Geosciences, University of Potsdam, Karl-Liebknechstr. 24/H25, Postfach 60 15 53, D-14476 Golm, Germany. (anke@alum.mit.edu)

J. Lee, Department of Geological Sciences, Central Washington University, 400 East 8th Avenue, Ellensburg, WA 98926, USA.

K. Sieh and B. P. Wernicke, Division of Geological and Planetary Sciences, California Institute of Technology, MS 100-23, 1200 East California Boulevard, Pasadena, CA 91125, USA.